A PARALLEL ALGORITHM FOR LARGE SCALE ELECTRONIC STRUCTURE CALCULATIONS

Thesis submitted for the degree of Doctor of Philosophy

of the

University of Edinburgh

by

DONALD JAMES MACLEOD

March 1988

ABSTRACT

The electronic structure problem is reviewed, and a self-consistent ab initio nonlocal pseudopotential calculation for AlAs is performed to illustrate the state of the art in the pseudopotential method. Application of the method to more complex materials, such as technologically advanced heterostructures, will necessitate very large basis sets and hence eigenproblems whose solution may not be feasible using the Householder algorithm on serial computers. With this in mind, a recursive algorithm for solving the matrix, the Lanczos algorithm, is presented. In the electronic structure context (providing local pseudopotentials are employed), this algorithm can be made faster by Fourier transforming a matrix-vector multiplication (i.e. a convolution) to a product of two vectors. This enhanced algorithm is especially advantageous when implemented on a parallel computer; this is demonstrated for the ICL DAP, a massively parallel array processor. Finally the DAP program is used to obtain non-self-consistent empirical bandstructures for $(GaAs)_n(AlAs)_n$ superlattices with n=1,2,4. The results are encouraging, but a machine with substantially increased memory would be needed to achieve self-consistency and to provide the arithmetic precision needed for the Lanczos algorithm to function well.

Acknowledgements

Science at the frontier nowadays incorporates so much complexity that it is seldom possible for an individual PhD student to function in complete isolation. Not claiming to be an exception to this, I must acknowledge the help of several people.

Firstly, my collaborators at Daresbury Laboratory ; Dr John Inglesfield and Dr Philip Sterne (now of the University of Maryland). They supplied me with the BHS code and instruction in its use, and later guided me through the "nitty-gritty" of solid state physics. Secondly, my academic supervisor, Professor David Wallace FRS, under whose aegis this work was done. As well as supplying many thought-provoking ideas and comments, he secured funding for the DAPs at Edinburgh and imbued me with a feeling for the future importance of parallel computing. Finally, Dr Richard Needs of Rank Xerox (Palo Alto) and Cambridge, for drawing my attention to the FFT speed-up. Two other members of the Edinburgh University Physics Department deserve special mention for alerting me to serious errors - Colin Farquhar and Professor Roger Cowley FRS. I am also in debt to Andrew Brass and Stephen Sheard for allowing me to use their respective FFT routines for the DAP (not easy things to write!).

On the computing side, I wish to thank the staff of the Edinburgh University Computing Service (particularly John Blair-Fish) for helping me in matters ranging from the arcane to the trivial. I also thank my employers since 1 October 1987, CAP Scientific Ltd, for the free use of an Apple Macintosh and a Laserwriter, on which this thesis was produced.

For valuable friendships I thank Charlie Wall and Colin Farquhar within the Physics Department, and Mark Bird, Bill Zachs and Mark Cropper elsewhere in the University. For some wonderful times in the mountains I will remember Adam Bennett, Martin Altebockwinkel, Clive Baillie and Quentin Mills (all Physics students of some sort).

Finally I dedicate this thesis to, and thank, my parents for their loving support (wine included).

To travel hopefully is a better thing than to arrive,
and the true success is to labour.

Robert Louis Stevenson

CONTENTS

1. INTRODUCTION

Since the inception of quantum mechanics, electronic energy band calculations have been recognised as an activity of overriding importance. They underpin most of solid state physics through their ability to calculate or explain most of the properties of materials. Furthermore, their predictions for materials yet to be exploited, or even made, can supply rich fuel for the engine of progress in device technology, especially in view of the advent of epitaxial growth techniques. We are now able to produce materials (such as semiconductor superlattices) whose properties are composition-dependent, and therefore tailorable. Unfortunately this field of so-called "bandstructure engineering" is in a fairly embryonic state due to the defects still inherent in electronic structure calculations.

The potential rewards are great however, since a tentative list of the results ultimately flowing from a bandstructure calculation (and subsequent total energy calculations) might run as follows : energy gaps, effective masses, charge densities (and hence bonding picture), mobility, density of states, stability under pressure, phases, atomic positions, phonon spectra, elastic constants, allowed optical transitions, heat of formation and stability of alloys, magnetic properties, power dissipation rates, frequency response, solubilities.

The process of obtaining the electronic structure is not an easy one, since the Schrodinger equation has to be solved for an assembly of interacting electrons of order 10^{23} in number. It is clearly impossible to derive a first-principles (or ab initio) potential for such a system, a classic example of a many-body problem. The problem is only tractable if it is reduced to that of one electron moving in an average potential due to all the others. Maximisation of the accuracy of this potential has long been the central problem of electronic structure work, and it has still not been satisfactorily solved, the stumbling block being the part of the potential due to electronic correlations. The most tractable description so far available for this part is the local density approximation (LDA). Symptoms of the remaining inadequacy of the LDA include incorrect energy gaps and inaccurate effective masses.

A wide variety of methods for tackling the electronic structure problem have appeared over the years. One of the most convenient ones, as described in chapter 3, is the ***ab initio*** pseudopotential, taken to self-consistency. The Schrodinger equation is cast in operator matrix form and solved for the low eigenvalues (energies) and eigenvectors (wavefunctions). A new potential, and thence a new Hamiltonian, is calculated from the wavefunctions using the density-functional formalism (chapter 2) and the cycle is repeated until the energies converge. Self-consistency is then said to be achieved.

The main focus of my work has been on algorithmic improvements. The motivation behind this is that electronic structure calculations (using any presently available method) for complex systems such as heterostructures would have very high computational costs. A good example of such a system is a semiconductor heterostructure, which consists of thin layers of different materials, and whose fundamental properties can be varied by adjusting the layer thicknesses. However, a proper treatment of even a single interface or surface is a big calculation. In the case of the pseudopotential method these costs are exemplified primarily by the significantly increased size of the Hamiltonian matrix, and magnified by the desirability of iterating to self-consistency (meaning that the matrix has to be solved many times). Faced with this sort of situation it is imperative to seek new algorithms, and at the same time exploit the latest advances in parallel computer architectures. The latter development represents the next step beyond the traditional serial computers, which suffer from the von Neumann bottleneck (i.e. only one data path between the single processing unit and the memory), and whose computing power is increasingly limited by the physics of the constituent material (either Si or GaAs) rather than by design. In parallel machines there are multiple processors, each with its own access to memory, and hence no bottleneck or (theoretical) upper limit to computing power.

The rate-determining step in the solution of the matrix is the reduction of the matrix to tridiagonal form (for which standard eigenvalue routines exist). This has usually been done with

the well-established Householder algorithm, but this has a computational cost (in CPU time) of order N^3, where N is the number of basis functions – plane waves for the pseudopotential method – in which the wavefunctions and the Hamiltonian are expanded. I perform a state-of-the-art pseudopotential calculation for the III-V semiconductor AlAs using this algorithm, and the results are given in chapter 3. For larger systems however, a N^3 algorithm is extremely slow. I have successfully implemented the Lanczos algorithm, which is less reliable than Householder but still very useful in certain circumstances, e.g. when only low eigenvalues are desired, as it is recursive and can be stopped when these have been obtained. In general the cost of this algorithm goes like that of a matrix-vector multiplication, that is to say N^2, but in the local pseudopotential method one can exploit the fact that the matrix only has N bits of information, being constructed from N basis functions. Therefore the matrix-vector multiplication in reciprocal space may be replaced by the Fourier transform of a vector-vector multiplication in real space. This increases the speed to NlogN, which I have confirmed. Details of both Householder and Lanczos algorithms (ordinary and fast) appear in chapter 4.

In recent years, computers with advanced architectures have become relatively widely available. Large vector processors such as the Cray are generally the most powerful of such machines, but are also expensive and in heavy demand. There exists a subset of scientific problems which may be handled more efficiently and cheaply on array processors which, although

smaller than a Cray, incorporate more intrinsic parallelism. In chapter 5, I argue that electronic structure calculations with pseudopotentials and the fast Lanczos algorithm fall into this category, and substantiate this claim with results on a relatively small array processor, the ICL DAP. On this machine the calculation of the eigenvalues of interest takes a time of order 1 minute per matrix solved, for all N up to a machine-dependent limit (32768 on the DAP). This speed is broadly equivalent to that of a Cray, but is achieved at less than 10% of the financial cost.

Unfortunately the limited storage of the DAPs at Edinburgh, combined with the apparent N-dependence of the point at which the Lanczos recursion process can be safely truncated, makes it impractical to obtain the eigenvectors. This precludes the implementation of self-consistency. As explained in chapter 5, I am therefore restricted to 'one-off' calculations. The most serious disadvantage of these is that the effects of charge transfer across interfaces cannot be accounted for, unless one adopts a perturbative formalism such as that due to Jaros. Furthermore, without the charge density (i.e. the eigenvector norm) it is not possible to study the bonding picture, or the confinement of states in the quantum wells formed by heterostructures. This disappointing state of affairs rules out the possibility of competition with state of the art calculations for heterostructures.

I therefore resort to empirical pseudopotentials to obtain the energy bands of the $(GaAs)_n(AlAs)_n$ system, for n=1,2 and 4. This system is an example of a superlattice with exciting applic-

ations in areas like high speed transistors and optoelectronics. The resulting bandstructures agree topologically with the few published results in this area, and are presented and discussed in chapter 6. In particular my results appear to confirm the recent important discovery that $(GaAs)_1(AlAs)_1$ has its conduction band minimum at the R point. It therefore has an indirect energy gap. The actual values I obtain for the gaps are too small, mainly due to the lack of selfconsistency (since the LDA is not used in my calculation).

Finally in chapter 7 I briefly criticise my work and make suggestions for future work.

The DAP code for my implementation of the fast Lanczos algorithm is given in an appendix.

2. THEORETICAL BACKGROUND

2.1. The electronic structure problem

Although it is essentially no more than solving the Schrodinger equation, the crystal electronic structure problem is rendered intractable to exact approaches by the vast numbers of electrons, and hence degrees of freedom, involved. Therefore approximations are necessary. Two approximations which have been found to be crucial - the adiabatic and one-electron approximations - are described below.

We will treat the nuclei with the core electrons bound to them as single entities, namely ions. The valence electrons (those from incomplete shells) are able to move through the solid when excited to the conduction bands. The non-relativistic Hamiltonian for the system of valence electrons (N_e in number) and ions forming the solid is :

$$H_0 = H_{el} + H_{ion} + V_{el\text{-}ion} \qquad (2.1)$$

where

$$H_{el} = \sum_j \left(-\frac{\hbar^2}{2m} \nabla_j^2 + \frac{1}{2} \sum_{j'}{}' \frac{e^2}{|\underline{r}_j - \underline{r}_{j'}|} \right)$$

is the purely electronic term,

$$H_{ion} = \sum_{\mu} \left(-\frac{\hbar^2}{2M_\mu} \nabla_\mu^2 + \frac{1}{2} {\sum_{\mu'}}' \frac{Z_\mu Z_{\mu'} e^2}{|\underline{R}_\mu - \underline{R}_{\mu'}|} \right)$$

is the purely ionic term and

$$V_{el\text{-}ion} = - \sum_{j,\mu} \frac{Z_\mu e^2}{|\underline{R}_\mu - \underline{r}_j|}$$

is the electron-ion interaction.

$\mathbf{r}_j$ and $\mathbf{R}_\mu$ denote electronic and ionic position vectors respectively, and M_μ denote ionic (effectively nuclear) masses. Primed inner sums exclude the case where the dummy equals the outer dummy.

We expect the ionic motion to be extremely slow relative to that of the electrons, and so the lattice dynamics (or electron-phonon interactions) may often be neglected as far as electron motion is concerned. This is achieved by means of the adiabatic (also called Born-Oppenheimer) approximation, which separates the electronic and ionic motions by writing the total wavefunction $\Phi(\mathbf{r},\mathbf{R})$ as a product of electronic and ionic wavefunctions, with $\mathbf{R}$ as a parameter in the electronic part :

$$\Phi(\underline{r}, \underline{R}) = \psi_{\underline{R}}(\underline{r})\, \eta(\underline{R}) \qquad (2.2)$$

This allows (2.1) to be rewritten as (H replacing H_o as it is no longer exact) :

$$H = T_{el} + T_{ion} + V_{\underline{R}}(\underline{r}) \qquad (2.3)$$

where the T's are the kinetic energies and $V_R(r)$ includes all contributions to the potential energy. T_{ion} does not act on the electronic wavefunction, so the electronic Schrodinger equation is :

$$\left[T_{el} + V_{\underline{R}}(\underline{r}) \right] \Psi_{\underline{R}}(\underline{r}) = E^{el}_{\underline{R}} \Psi_{\underline{R}}(\underline{r}) \qquad (2.4)$$

The remaining part of the problem gives the lattice dynamics, which we do not discuss here. Dropping the ionic position label **R**, and noting that ψ is a function of all N_e electron coordinates, we rewrite (2.4) as :

$$\sum_j \left(-\frac{\hbar^2}{2m} \nabla_j^2 + V_{el\text{-}ion}(\underline{r}_j) + \frac{1}{2} \sum_{j,}{}' \frac{e^2}{|\underline{r}_j - \underline{r}_{j'}|} \right) \Psi(\underline{r}_1, \cdots \underline{r}_{N_e}) = E \Psi(\underline{r}_1, \cdots \underline{r}_{N_e}) \qquad (2.5)$$

E is the total energy of the electron gas in the presence of a fixed configuration of ions. We may remark here that an important new calculational technique (Car & Parrinello, 1985) permits the inclusion of ion dynamics alongside a fictitious electron dynamics and relaxes the system to the equilibrium ionic geometry, as well as the correct eigenenergies, through 'timestepping', as in molecular dynamics.

Because of the different **r**'s in the third term, the electron-electron interaction, equation (2.5) is not separable in the coordinates $\mathbf{r}_j$. A gas of interacting bosons would have the

same problem, but would be amenable to statistical mechanical techniques combined with quantum field theory, whereas fermion fields anticommute and cannot be represented by real numbers on a computer. To make progress for our electron gas we need the one-electron approximation, in which we write the total wavefunction as a product of one-electron wavefunctions $\psi_i(\mathbf{r}_j)$, $j=1,\ldots N_e$. A simple product (the original suggestion of Hartree) would not have the antisymmetry with respect to interchange that is required to satisfy the Pauli exclusion principle, so we postulate linear combinations of products in the form of a Slater determinant :

$$\Psi(\underline{r}_1,\ldots\underline{r}_{N_e}) = \frac{1}{\sqrt{N_e!}}\begin{vmatrix} \psi_1(\underline{r}_1) & \psi_1(\underline{r}_2) & \cdots & \psi_1(\underline{r}_{N_e}) \\ \psi_2(\underline{r}_1) & \cdot & & \cdot \\ \cdot & & \cdot & \cdot \\ \cdot & & & \cdot \\ \cdot & & & \cdot \\ \psi_{N_e}(\underline{r}_1) & \cdots & & \psi_{N_e}(\underline{r}_{N_e}) \end{vmatrix} \qquad (2.6)$$

Exchange of any 2 columns changes the overall sign, as required. (Note that the exact wavefunction would consist of an infinite series of N_e x N_e determinants). Taking (2.6) to be the wavefunction, we minimise the expectation value of the energy, which is given by the expression $\langle\psi|H|\psi\rangle/\langle\psi|\psi\rangle$. Introducing Lagrange multiplier parameters ε_i, we arrive at the N_e Hartree-Fock equations (see, for example, Slater 1974) :

$$\left[-\frac{\hbar^2}{2m}\nabla^2 + V_{el\text{-}ion}(\underline{r}) + \sum_j e^2 \int \frac{\psi_j^*(\underline{r}')\,\psi_j(\underline{r}')\,d^3r'}{|\underline{r}-\underline{r}'|} \right] \psi_i(\underline{r}) \cdots$$

$$- \sum_j e^2 \psi_j(\underline{r}) \int \frac{\psi_j^*(\underline{r}')\,\psi_i(\underline{r}')\,d^3r'}{|\underline{r}-\underline{r}'|} = \epsilon_i \psi_i(\underline{r}) \qquad (2.7)$$

From left to right the terms are the kinetic energy, the potential due to the ions, and the Hartree (pure Coulombic) and exchange potentials. The latter two are collectively called the 'screening' potential since the interelectronic interactions are reducing, or screening, the ionic potential. The theorem of Koopmans (1933) allows us to identify the parameters ε_i as the one-electron energies. The proof evaluates total energies using Slater determinants of N_e-1 and N_e functions respectively, showing that the difference is equal to the ε parameter for the extra (N_e'th) state possessed by the larger determinant. This theorem is therefore only valid for a total wavefunction of the form (2.6).

The last term on the left of (2.7) is clearly nonlocal. This is the exchange term, which arises from the electron correlations required to conform with our choice of antisymmetric wavefunction. Primed sums are not needed now since the self-energy (the case i=j) cancels exactly between the Hartree (pure coulombic) and exchange potentials. The equations (2.7) have to be solved self-consistently because the Hartree and exchange potentials depend non-linearly on the wavefunction ψ; in

particular, the Hartree term depends explicitly on the charge density :

$$\rho = \sum_j \psi_j^*(\underline{r}) \psi_j(\underline{r}) \qquad (2.8)$$

The nonlocality of exchange makes approximate treatments necessary for all but the simplest systems. Such treatments are usually based on the exactly soluble case of a free electron gas with a uniform positive jellium background. Here, the ψ's reduce to plane waves and the exchange potential is found to be proportional to $\rho^{1/3}$ (e.g. Slater, 1974). This can be understood by means of a simple argument in electrostatics involving the exchange "hole" (really an average reduction in charge density) induced around each electron. The radius R of this spherical region has to satisfy $\frac{4}{3}\pi R^3 \rho = e$, where ρ is the density of charge of the same spin as the electron. The potential of the electron at the centre, due to the sphere of charge, varies as 1/R and hence as $\rho^{1/3}$. The exact proportionality depends on the electron wavevector, and different values were suggested by Slater and by Kohn and Sham. Slater also suggested varying this constant of proportionality in an attempted simulation of the further corrections needed to improve the Hartree-Fock approximation, and this idea gave rise to the moderately successful X-α method (Slater, 1972), still used to this day.

Löwdin suggested that such corrections to represent 'all energy terms beyond Hartree-Fock' be known collectively as the correlation energy, and we now discuss this. It will aid our

exposition to introduce the pair distribution function $g_{12}(r)$, defined as the probability that there is an electron in spin state 1 at r if there is one in spin state 2 at r=0. Now, the inclusion of the exchange term in the Hartree-Fock equations is equivalent to the statement that $g_{\uparrow\uparrow}(0)=0$, i.e. electrons with the same spin never occupy the same state. Also, for large N_e, $g_{\uparrow\uparrow}$ and $g_{\uparrow\downarrow}$ both tend to 1/2 at large r, if the material is not magnetically ordered. The failure of the Hartree-Fock approximation is apparent when we look at $g_{\uparrow\downarrow}$ which is claimed to be 1/2 for all r, i.e. electrons with opposite spins should not correlate in any way. But Coulomb correlations (which are spin-independent) produce a region of charge depletion associated with each electron, and by allowing opposite-spin repulsions to contribute alongside same-spin repulsions to this "exchange-correlation hole", the real system has a total energy which is lower than that of the system described by the Hartree-Fock equations. That is to say, we allow $g_{\uparrow\downarrow}<1/2$ at small r in order to achieve the state of minimum total energy. It is this relaxation of $g_{\uparrow\downarrow}$ that gives rise to the correlation energy. This change also causes the kinetic energy to adjust.

A precise mathematical treatment of correlation involves the techniques of many-body perturbation theory, which are complicated and laborious to apply in practice. It is also unsatisfactory to stick such a treatment onto the Hartree-Fock formalism in an ad-hoc way, or to make guesses as in Slater's X-α method. What is needed is a framework which treats both exchange and correlation together in a systematic approximation.

This is provided by density functional theory, discussed in the next section.

Before moving on we remark that the treatment so far has been nonrelativistic. Relativistic effects are sometimes significant, especially in the neighbourhood of heavy atoms, and this will be taken into account later.

2.2 Density functional theory

The Hartree-Fock approach to a many-electron system is limited by its initial assumption about the nature of the wavefunction. Density functional theory makes no such assumption. Instead it asserts that the total energy of the electron gas is a unique functional $E[\rho]$, where ρ is the ground state charge density. Since the wavefunction is functionally related to the energy via the Schrodinger equation, it follows that all the ground state quantum mechanical properties of the system are also functionals of the density. This remarkable theorem was proved by Hohenberg and Kohn (1964), using the technique of reductio ad absurdum. That is to say, they postulated the existence of two different external potentials (and hence different ground states) corresponding to the same charge density, and showed that this led to a contradiction. This theorem means that we can write the ground state energy as :

$$E[\rho] = \int V_{ion}(r)\rho(r)\,d^3r + T[\rho] + \frac{e^2}{2}\int\frac{\rho(r)\rho(r')d^3r'}{|r-r'|} + E_{xc}[\rho] \qquad (2.9)$$

The first term on the right is the potential due to the ions or nuclei (or in general, the external potential) and the remaining 3 terms (kinetic, electrostatic and exchange-correlation) constitute a universal functional for the electron system, valid with any external potential. The correct charge density is the one which minimises (2.9). We now vary (2.9) with respect to the density and obtain :

$$\int \delta\rho(r)\left[\frac{\delta T[\rho]}{\delta\rho(r)} + V_{ion}(r) + e^2\int\frac{\rho(r')d^3r'}{|r-r'|} + \frac{\delta E_{xc}[\rho]}{\delta\rho(r)}\right]d^3r = 0 \qquad (2.10)$$

The imposition of the constraint that the number of particles remain constant :

$$\int \delta\rho(r)\,d^3r = 0 \qquad (2.11)$$

yields the result that the contents of the square brackets in (2.10) must equal a constant, to be identified as the chemical potential. The same result would be obtained for a collection of non-interacting electrons moving in an external effective potential given by :

$$V_{eff}(r) = V_{ion}(r) + e^2\int\frac{\rho(r')d^3r'}{|r-r'|} + V_{xc}(r) \qquad (2.12)$$

in which $V_{xc}(r) = \dfrac{\delta E_{xc}[\rho]}{\delta\rho(r)}$

Therefore it is valid to lump all the interaction physics into an effective potential and to represent exchange/correlation effects by a local potential V_{xc}. The solution of the many-electron problem thus reduces to that of a (fictitious) one-electron Schrodinger equation, whose eigenfunctions ψ_i are required to conform with the charge density :

$$\rho = \sum_{occ\, i} |\psi_i|^2 \qquad (2.13)$$

which minimises the energy functional. The sum is over all occupied states. With (2.13) substituted for ρ, and an appropriate formulation for the kinetic energy functional T, we can vary (2.9) with respect to the ψ_i's to yield the N_e Kohn-Sham equations (Kohn & Sham, 1965) :

$$\left[-\frac{\hbar^2}{2m}\nabla^2 + V_{ion}(r) + e^2 \int \frac{\rho(r')\, d^3r'}{|r-r'|} + V_{xc}(r) \right] \psi_i(r) = \epsilon_i \psi_i(r) \qquad (2.14)$$

Like the Hartree-Fock equations, (2.13) and (2.14) have to be solved self-consistently. The difference is that the Kohn-Sham equations are in principle exact. There is no theorem like that of Koopmans for the Hartree-Fock parameters, but the ε_i in (2.13) can still be regarded as approximations to the single-particle energies of exact many-body theory. This is because the Kohn-Sham equations and the many-body quasiparticle equations (see e.g. Pickett & Wang, 1984) are of similar form, differing only

in that the latter contain a nonlocal energy-dependent operator (the 'mass operator') in the exchange-correlation term. Their eigenfunctions are also very similar at low energies, especially in a semiconductor. Another convincing piece of evidence is that ε for the highest occupied state is equal to the Fermi energy at 0K, as it should be.

Before solving the equations we need to specify an approximation to V_{xc}. Unfortunately the Hohenberg-Kohn theorem is only an existence theorem and gives no clue to the functional form of V_{xc}. We expect however that complex details of the system will be unnecessary for a reliable approximation, since V_{xc} is a local function which has to serve for all the eigenstates. The method usually chosen is the local density approximation (LDA), which takes V_{xc} to be that of a homogeneous electron gas evaluated at the **local** density. (The exchange-correlation energy as a function of density has been calculated for a homogeneous gas by many workers, e.g. Ceperley & Alder, 1986). The LDA is accurate enough if the density is slowly varying. In fact it has been used with some success in situations like surfaces, where the charge distribution is grossly inhomogeneous.

We should now point out a significant flaw in density functional theory. Self-consistent calculations for non-metals using DF theory and the LDA invariably give an energy gap which is too small, typically by 20-90%. One might say this is because DF theory is only valid for the ground state, whereas the energy gap depends on an excited state (the lowest conduction band) ; but

it is more subtle than that because the gap can actually be expressed in terms of three ground state total energies, denoted by E_M (for M electrons filling the valence bands), as follows. Removing one electron from the highest valence band to infinity changes the energy of an N-electron system from E_N to E_{N-1}, so the minimum needed (the ionisation energy I) is $E_{N-1}-E_N$. Introducing an electron from infinity to the bottom of the conduction band changes the energy by E_N-E_{N+1}, called the electron affinity A.

The gap is equal to I–A :

$$E_g = E_{N+1} + E_{N-1} - 2\,E_N \qquad (2.15)$$

The (erroneous) Kohn-Sham gap turns out to be equal to (2.15) if V_{xc} is any continuous function of N, as would be given by the LDA, because the four exchange/correlation terms on the right will cancel out, assuming N sufficiently large. Thus the gap error is not caused by the LDA. To cure the discrepancy in the energy gap it is necessary to add a nonconstant correction ΔV_{xc}, reflecting a discontinuity in V_{xc} at that value of N which fills the occupied states. In other words the exchange-correlation potential undergoes a jump when one electron is added to the insulating (filled valence-band) system. This correction amounts to the calculation of a nonlocal (i.e. energy-dependent) single-particle self-energy, $\Sigma(r,r',E)$ and is currently the focus of active research. Pickett and Wang (1984) proposed a 'quasiparticle LDA' (QPLDA) formalism based on an approximation to Σ, the 'GW'

approximation (Hedin & Lundqvist, 1969), which is proportional to $\delta(r-r')$, i.e. local in space. However this is still inadequate, as it has been shown (Godby et al., 1986) that the range of spatial nonlocality in Σ is comparable to the wavelength of the wavefunctions, so that a fully nonlocal approximation is required. Godby et al. (1987) have modelled self-energies by a function of the form :

$$\Sigma(\underline{r},\underline{r}',E) \approx \frac{1}{2}\left(f(\underline{r})+f(\underline{r}')\right) g(|\underline{r}-\underline{r}'|)\, h(E) \qquad (2.16)$$

where f,g and h are functions to be fitted to the quasiparticle self-energy, previously evaluated in the GW approximation.

In summary, in this chapter we have described the electronic structure problem and seen that it is still some way from being fully resolved theoretically. This state of affairs is mainly due to the continuing omnipresence, in current band-structure methods, of approximate treatments of electron correlation.

3. PSEUDOPOTENTIALS - THEORY AND APPLICATION

3.1. History

The pseudopotential method is one of the most important bandstructure techniques as well as being arguably the simplest one to use. Its outstanding success in recent years is firmly rooted in the density functional formalism, which allowed the construction and implementation of powerful ab initio pseudopotentials to take place. Since most of the work reported in this thesis had to be done with the older empirical pseudopotentials, we adopt a historical discussion which covers these first.

The Hamiltonian operator and its eigenfunctions have to be represented for computational purposes as expansions in terms of some set of orthonormal basis functions. This produces a secular equation for the energies and wavefunctions. The simplest such set is plane waves, i.e. a Fourier expansion. But in a real solid the valence wavefunctions (the only ones of real interest) are highly oscillatory around ionic sites in order to be orthogonal to the highly localised wavefunctions of the electrons bound to the core, and are smooth in the interstitial regions. The representation of this schizophrenic nature by plane waves is computationally unfeasible; even for a light atom with a relatively weak (or "soft") core potential one would get a secular equation of order 10^6. Heine (1970) has supplied a back-of-envelope argument for this number, using aluminium. Its 1s core state is positive

everywhere and falls from a maximum at the origin to zero at about 2/13 atomic units (a.u.). To be orthogonal to it any valence state has to have a node around 1/13 a.u. and so we need plane waves down to a wavelength a bit less than this, say 1/16 a.u. This is 1/100 of the atomic diameter of 6 a.u., which is the sort of wavelength associated with valence states in the interstitial regions. Thus a grid of 100 reciprocal lattice vectors is needed in each of 3 dimensions, making a total basis of 10^6.

There are two ways of surmounting this difficulty. One can either choose a more complex basis set, or one can modify the potential to give a plane-wave-expandable wavefunction with the same physical content as the real one. The first line of attack spawned many more sophisticated basis functions. For example, the LAPW (linear augmented plane wave) method uses expansions in atomic orbitals in the core regions matched up to Fourier expansions outside. Such methods give secular equations of order 10^2, but the computer codes tend to be complex.

The second approach is the pseudopotential, in which the singularities in the potential at the ionic sites are cut off to give a relatively smooth pseudopotential, for which a Fourier expansion is feasible. Thus the troublesome core states and the deep potentials which bind them are eliminated. The method requires that the electron states be capable of unambiguous division into core states, assumed to be the same as in the free atom, and valence states. This is occasionally impossible ; in the first row transition metals for example, the 3d valence states

are rather atomic-like, so a method like LAPW would be superior to pseudopotentials here.

The "pseudopotential equation" is as follows, adopting Dirac notation :

$$-\frac{\hbar^2}{2m}\nabla^2|\phi\rangle + V_{ps}|\phi\rangle = E|\phi\rangle \qquad (3.1)$$

The only requirement is that E correspond to the real one-electron eigenvalue; therefore there are arbitrarily many ways of specifying both the pseudopotential V_{ps} and the pseudowave-function ϕ. Note that V_{ps} is screened, i.e. it is a total effective potential, like V_{eff} in (2.12). Prior to the 1970's pseudopotentials followed two parallel lines of development, empirical and non-empirical (or ab initio).

Empirical potentials (reviewed by Cohen & Heine, 1970) are less rigorous but quite successful in the short term. In one type the total potential is represented by just a few terms in a Fourier expansion, with their coefficients adjusted to agree with some experimentally determined features of the energy bands, esp-ecially the topology and energy gaps. This is the type I use for the work in chapter 6 (q.v). In the other type, called the "model potential", the bare ion potential is simulated by an adjustable constant discontinuously joined to a Coulomb tail (see Figure 3.1), and this could be screened by dividing by a dielectric function. Taking advantage of the separation of ionic and screen-ing terms, this type could also be taken to selfconsistency,

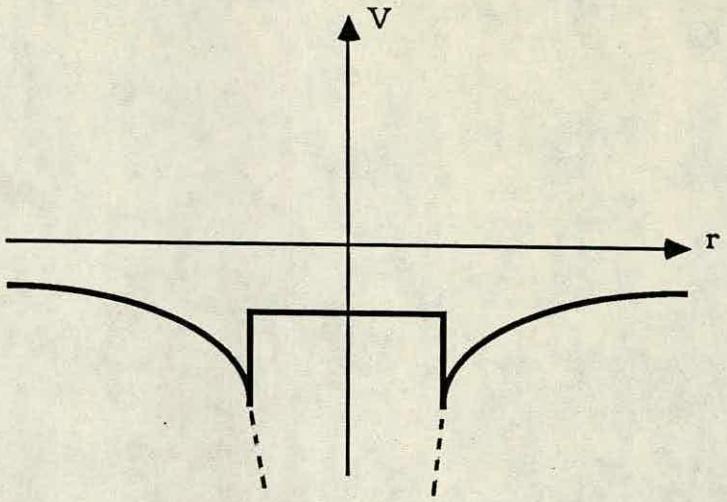

Figure 3.1. The model pseudopotential of a bare ion

computing new screening potentials from charge densities in a density-functional framework. This method was very successful for bulk bandstructures, but it was found that model potentials were not transferable, meaning that they could not be employed in different geometries such as surfaces or interfaces, where many extra Fourier components were required to represent the overall potential. The main problem is the discontinuity, which causes slow convergence in Fourier space. Another problem is the non-locality caused by slightly different constants being required to fit the potential to states with different quantum number ℓ ; in addition these constants prove to be weakly energy-dependent.

Ab initio (first principles) potentials were for a long time worse than empirical ones. They were certainly not transferable and could not even be taken to selfconsistency, due to lack of norm-conservation, i.e. incorrect valence charge densities. This is well illustrated by the first ab initio pseudopotentials. These

took their cue from the orthogonalised plane wave (OPW) method, which uses basis functions orthogonalised to the core states $|c\rangle$:

$$|opw\rangle = |pw\rangle - \Sigma_c |c\rangle\langle c|pw\rangle$$
$$= (1 - P)|pw\rangle \qquad (3.2)$$

where P is the projection operator $\Sigma_c|c\rangle\langle c|$. Just as the humble plane wave yields a superior basis function (for valence states) when the core states are projected out, so we can reasonably assume the existence of some smooth function ϕ which would yield the exact valence wavefunction ψ when treated in an analogous fashion :

$$|\psi\rangle = (1 - P)|\phi\rangle \qquad (3.3)$$

Phillips & Kleinman (1959) constructed pseudopotentials based on this formalism. However, it is clear from (3.3) that $\langle\phi|\phi\rangle \neq \langle\psi|\psi\rangle$. In practice the pseudo charge density would be 5-10% too high. Incorrect charge densities give incorrect screening potentials and a selfconsistent calculation would never converge to the correct energies.

3.2. Ab initio pseudopotentials that work

In 1979 a major breakthrough occurred when the first norm-conserving ab initio pseudopotentials were constructed (Hamann et al, 1979). With these potentials the real and pseudo wavefunctions are identical beyond some chosen "core" radius r_c, the real and pseudo charge densities are the same for $r > r_c$ for each valence state (norm-conservation), and the logarithmic and energy derivatives of the real and pseudo wavefunctions agree for $r > r_c$ (ensuring accurate simulation of the scattering properties of the real ion core). The simultaneous fulfilment of these 3 conditions guarantees excellent transferability to new geometries and/or chemical environments (including impurities and defects), situations which will shift the eigenenergies away from their atomic levels. Effectively the ion core is replaced by a black box with the same external properties. Transferability occasionally fails for low and high energies, due to divergence of the real and pseudo logarithmic derivatives.

Three years later a table of such pseudopotentials, for all elements up to plutonium, was published (Bachelet, Hamann & Schlüter, 1982 - hereafter BHS). As well as being norm-conserving, and therefore usable, these potentials are also nonlocal and relativistic. In this context, "nonlocal" means that the angular momentum quantum number ℓ is incorporated, so that electrons in s,p,d,... states feel slightly different potentials. This feature is desirable (and essential for a few elements, e.g. oxygen) as it

makes the potential much more realistic, but it makes efficient computer coding more difficult, as we shall see in section 5.2. For full details of the BHS construction method, their paper should be consulted; a brief summary is given here.

The essence of the construction is to find some smooth wavefunction ϕ which matches ψ for all $r > r_c$. Then the corresponding potential can be obtained by inverting the Schrödinger equation. Firstly the Kohn-Sham equations (2.14) are made fully relativistic - as far as one-electron potentials are concerned - by substituting a Dirac equation (in fact a Schrödinger-like approximation to it which is accurate for valence electrons outside r_c) for each Schrödinger equation, and then solved selfconsistently. The singularities of the resulting potential are cut off by an artificial construction, and the radial Schrödinger equation is then solved with this new potential. The resulting eigenfunctions are normalised to coincide with ψ for $r > r_c$, and a term dependent on $r^{\ell+1}$ is added for $r < r_c$. We now have the pseudowavefunction ϕ. This introduction of nonlocality to the so-called core region does not affect the norm-conservation outside r_c. Finally they get the potential by analytic inversion of the Schrödinger equation containing ϕ and its eigenvalue. This inversion can only be done if ϕ is nodeless, so r_c is not a completely free parameter - its lower limit is the outermost node in the true wavefunction ψ. To make it useful for selfconsistent calculations, the potential is unscreened by subtraction of Hartree and exchange-correlation potentials (which are calculated from the pseudo charge density).

The LDA, with correction factors to account for relativistic QED effects (McDonald & Vosko, 1979), is used for the exchange-correlation potential. The final bare ion pseudopotentials are then fitted to standard functions (erfs and gaussians) for tabulation.

The regurgitation of the potential from its tabulated parameters can be an unstable process in single precision arithmetic. Different computers will produce different potentials. This problem is greatly reduced in double precision, which should therefore be regarded as essential here.

3.3. Selfconsistent calculation for AlAs

The starting point for this section is a package of two computer programs for performing selfconsistent pseudopotential calculations. It was originated by Schlüter around 1972, presumably for use with empirical potentials, and has since been modified by others. The most important modification (in 1982) added several subroutines for setting up and using the powerful Bachelet-Hamann-Schlüter potentials discussed in the previous section. I use this package to calculate the BHS bandstructure of AlAs, a III-V semiconductor for which relatively few calculations have been done. This work forms a sequel to a similar calculation for GaAs by P.Sterne (unpublished).

We first describe the general features of the computer implementation. The potentials and wavefunctions are expanded in terms of N plane waves exp(i**G**.**r**) centred on a user-chosen point **k** in the Brillouin zone, leading to this secular equation :

$$\left[(\underline{k}+\underline{G})^2 \delta_{\underline{G}\underline{G}'} + \langle \underline{k}+\underline{G} | V_{ion} + V_{scr} | \underline{k}+\underline{G}' \rangle \right] \phi = E\phi \quad (3.4)$$

Henceforth, atomic units ($\hbar$=2m=1, e^2=2, E in rydbergs; 1 Ry=13.6 eV) are employed. The two programs run in alternation; one (PBS) sets up and solves the N x N secular equation and the other (CHAT) calculates a new screening potential from the PBS eigenvectors. V_{ion} sits unchanged in PBS throughout, the new V_{scr} (or, for stability, a mixture of new and old V_{scr}'s) being added to it on each iteration. The process is initiated with either a screening potential from a system similar to the one under study or a screened empirical pseudopotential (replacing the BHS potential for the first iteration only). The calculation terminates when the eigenvalues on two successive iterations are the same to within the desired accuracy, typically 0.01 eV or less.

During the quest for selfconsistency each iteration must be performed on a set of special **k**-points, although the same set does not have to be used for all the iterations. Such a set has the property that the integration over the Brillouin zone of any periodic function of wavevector - in our case, the charge density - is accurately given by some weighted sum of its values at the special points. These points and their weighting factors are systematically chosen from "shells" of symmetry-equivalent

lattice points, and by including enough shells, any accuracy may be achieved (Chadi & Cohen, 1973; Monkhorst & Pack, 1974). On achieving a converged potential, one can run PBS separately at any number of **k**-points, usually along the crystal's symmetry lines, to generate the desired bandstructure.

We now comment on the screening potential calculation in CHAT. The Hartree part is easy, being obtained exactly from a Fourier-transformed Poisson equation :

$$V_H(\underline{G}) = \frac{4\pi\rho(\underline{G})}{G^2} \qquad (3.5)$$

The exchange-correlation part is the only significant approximation of the whole calculation. As long as ρ is slowly varying, this is well described by the local density approximation (LDA) :

$$V_{xc}(\underline{r}) = \frac{\delta E_{xc}[\rho(r')]}{\delta\rho(r)} \simeq \frac{\delta}{\delta\rho(r)}\int \epsilon_{xc}(\rho)\,\rho(r)\,d^3r = \frac{d(\epsilon_{xc}\rho)}{d\rho} \qquad (3.6)$$

where ϵ_{xc} is the exchange-correlation energy per particle of a uniform electron gas of density ρ. Several interpolation formulae exist for ϵ_{xc} and I use the most popular, that of Hedin and Lundqvist (1971) :

$$\epsilon_{xc} = -e^2\left(\frac{3\rho}{\pi}\right)^{1/3}\left[1+\left(\frac{4\pi^2}{9}\right)^{1/3}\frac{r_s}{2}\ln\left(1+\frac{r_s}{21}\right)\right] \qquad (3.7)$$

where r_s is a measure of density : $\frac{4}{3}\pi r_s^3 = \rho\Omega$

Ω is the unit cell volume. Note that V_{xc} is evaluated in real space, making Fourier transforms necessary.

The three important factors governing the overall computing time are the number of plane waves N, the number of special **k**-points, and the choice of algorithm for reducing the matrix to tridiagonal form. For a semiconductor, $N \sim 300$ is found from experience to be the smallest practicable basis for BHS pseudopotentials. Either 2 or 10 special **k**-points are used (Chadi & Cohen, 1973). Matrix algorithms will be discussed in the next chapter; PBS uses the Householder algorithm for tridiagonalisation. My calculations for AlAs were performed on a NAS 7000, a fast serial computer on which each iteration takes about 3.5 minutes per **k**-point. Thus a 10-point iteration takes over 30 minutes. The PBS program accounts for nearly all of this time.

As the BHS potential was derived from first principles, the only experimental information utilised by my AlAs calculation is the lattice constant a, which is 5.662Å at 300K (Weast, 1981), and the symmetry of the lattice, which is face-centred cubic. The unit cell contains two atoms, one Al at (0,0,0) and one As at (a/4,a/4,a/4).

A basis set of about 300 plane waves was used throughout, with the capability of including a further 100 via Löwdin perturbation (Löwdin, 1951). This form of perturbation involves adding to every Hamiltonian matrix element H_{nm} the following quantity:

$$\sum_{\gamma=N+1}^{\Gamma} \frac{H_{n\gamma} H_{\gamma m}}{E - H_{\gamma\gamma}} \qquad (3.8)$$

where Γ is the total number of basis functions, 400 in our case. To use (3.8) without prior knowledge of the eigenvalues, E has to be replaced by the kinetic energy (on the diagonal) or some estimated average eigenvalue (off the diagonal).

Since GaAs and AlAs are chemically similar substances with lattice constants equal to within 2%, the calculation could be safely initiated with a converged GaAs screening potential, and 5 iterations were then done at the 2 special points $\mathbf{k}$=(1/4,1/4,1/4) and (3/4,1/4,1/4) in units of $2\pi/a$. This yielded eigenvalues converged to 0.01 eV. To improve the accuracy of screening even further, 3 more iterations (the last one incorporating Lowdin perturbation) were done at a set of 10 special points. The 2- and 10-point sets do not intersect so eigenvalues could not be compared. The screening potentials do not depend on $\mathbf{k}$ so they were compared and found to differ slightly between iterations 5 and 8, mostly due to the extra iterations. The final converged potential was used to generate bandstructure along L-Γ-X. Γ is the origin of $\mathbf{k}$-space and X=(π/a,0,0) and L=($\pi/2a$,$\pi/2a$,$\pi/2a$) lie on the boundary of the Brillouin zone. The resulting plot of E against $|\mathbf{k}|$ is shown in Figure 3.2, with the usual convention that the zero of energy is set at the top of the valence band. AlAs has 8 valence electrons per unit cell, hence the 4 valence bands. Only 3 are visible since the top 2 are exactly degenerate (by time-reversal symmetry).

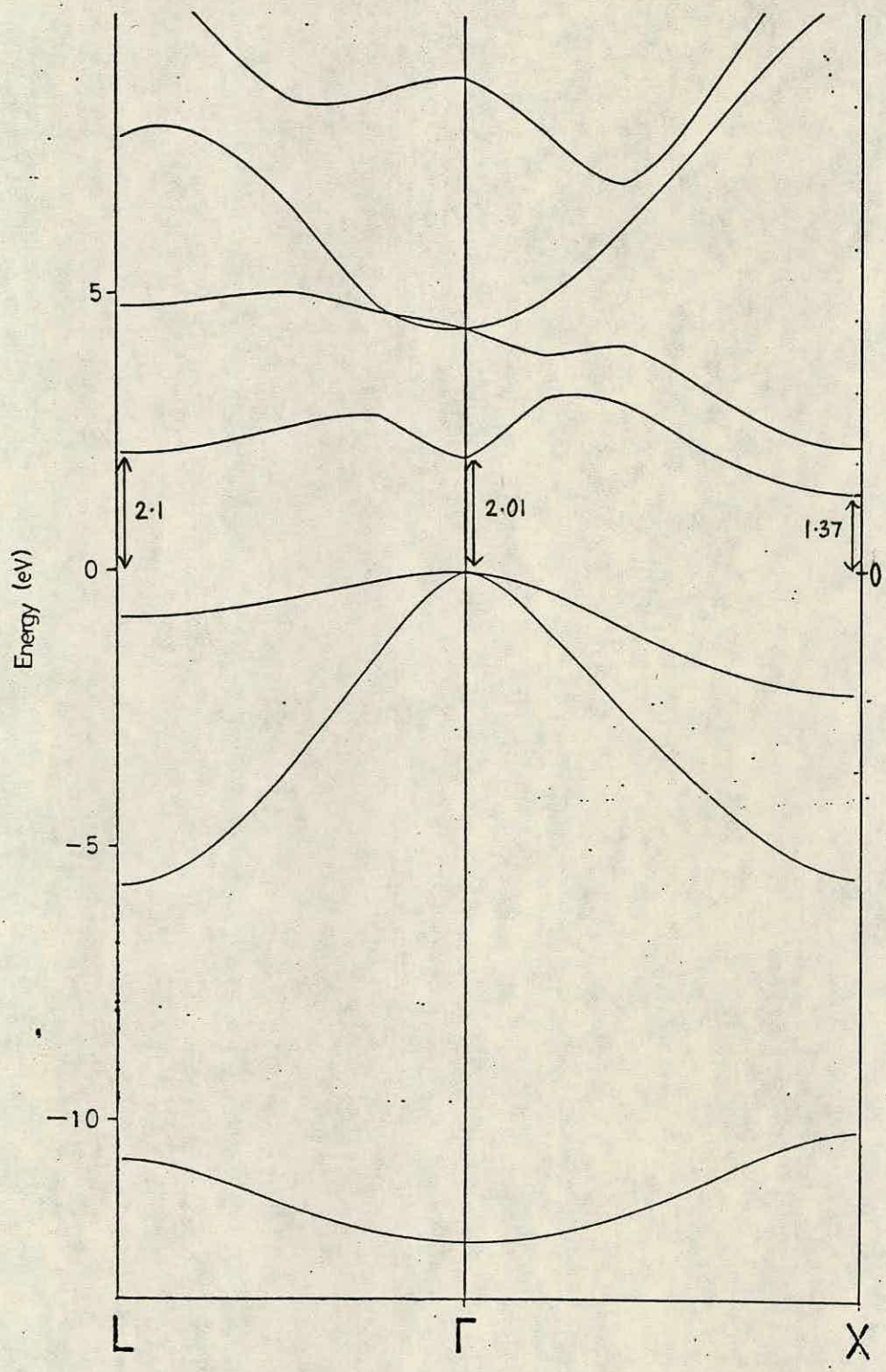

Figure 3.2. Bandstructure of AlAs along L-Γ-X

The energy at (0.95π/a,0,0) was found to be 0.01 eV above that at X, indicating that the conduction band minimum lies either at X or within 0.05π/a wavevector units of it, as expected.

This calculation is apparently the best yet performed for AlAs from first principles, since the only comparable one (Froyen & Cohen, 1983) used the same norm-conserving construction, but starting from a simple Schrodinger equation instead of our Dirac equation. Relativistic effects are manifested by the differences between the energy gaps obtained with BHS and Froyen-Cohen potentials. These differences, $E_g(FC)-E_g(BHS)$, are 0.28 eV for AlAs and 0.55 eV for GaAs, the latter change being larger because Ga is heavier then Al, and so electrons in the Ga-like bottom conduction band of GaAs are more relativistic. Energy gaps can only be compared in this way because the top valence band is As-like in both materials and so BHS/Froyen-Cohen differences in gaps are due mostly to conduction band effects.

We also remark that the lowest conduction band (denoted by Γ_{1c} in this system) is the hardest to converge. On the basis of Froyen & Cohen's experience we expect this to be the only state that will change if we take N > 330 and even then by no more than about 0.1 eV. Using the converged AlAs potential, I tried one further iteration with half the basis ($N \sim 160$) and found that all the states changed by less than 2% from those in Figure 3.1, with the exception of Γ_{1c} which changed from 2.01 eV to 2.47 eV. This shows that this particular state is not yet stable.

Finally we discuss how these results could be compared with experiment. The perfection in recent years of the technique of angle-resolved photoemission (ARUPS) has yielded full E-**k** curves from experiment for the first time. This method uses the photoelectric effect; the material is bombarded with high-energy photons and the angles of emission θ and energies of the photoelectrons are measured. The electrons' initial states are found by subtracting the photon energy from the observed final energies, and the wavevector **k** is obtained directly from θ by momentum conservation. Thus a bandstructure can be generated.

Recent ARUPS experiments for six III-V semiconductors (Williams et al, 1986) unfortunately do not include AlAs. If an experimental bandstructure for AlAs were available, we would expect it to be in good agreement with the best empirical pseudopotential calculations (e.g. Chelikowsky & Cohen,1976) but to disagree with our BHS calculation in one important respect. The general shape of our calculated bands is likely to be accurate, but as discussed in section 2.2, the energy gap is too low because the LDA fails to account for the discontinuous nature of the exchange-correlation energy. In the case of AlAs our gaps are about 50% too low (which is typical) when compared to those measured by optical absorption (Monemar, 1973). For the direct gap at Γ we have 2.01 eV (experiment 3.03 eV) and for the indirect gap from Γ to X 1.37 eV (experiment 2.15 eV). Froyen & Cohen did slightly better, obtaining a direct gap of 2.29 eV. It is not clear how their calculation could give a better gap.

At least we can correctly identify AlAs as an indirect-gap material; however we cannot rely on doing this for other materials as the self-energy correction ΔV_{xc} that we have omitted (see section 2.2) can sometimes vary over the Brillouin zone.

We conclude this chapter by observing that the pseudopotential has the advantage over other ab initio methods of being simple to use, yet still capable of giving excellent results. This very simplicity makes it the logical choice for more complex systems such as heterostructures. But we have seen that a self-consistent calculation (using 300 basis functions) for a simple bulk material consumes over 2 hours of serial computer time altogether. This would scale roughly as the cube of the basis size, given the matrix algorithm that we used (Householder). However, by a change of algorithm it is possible to greatly reduce this problem; and by changing from a serial to an appropriate parallel computer it is even possible to completely eliminate the dependence of CPU time on basis size. Chapters 4 and 5 respectively describe how these two objectives may be achieved.

4. MATRIX ALGORITHMS

4.1. Householder algorithm

Most methods for the solution of small matrices work by reducing the symmetric (or Hermitian if complex) matrix to a simplified standard form - usually tridiagonal - by a sequence of unitary transformations. The computational costs invariably scale as N^3, N being the order of the matrix. The most popular one is the Householder algorithm (Householder 1958). This was the choice of Schlüter for his pseudopotential code, where it is used for the Hermitian matrix H. We now outline its operation.

The idea is to apply successive unitary transformations P^rHP^r, (r=1,2,...N-2) in order to zero each column-row pair in turn except for elements on the 3 central diagonals (which only get modified), thus giving a tridiagonal end product. This can be accomplished by the following choice :

$$P^r = I - 2\underline{w}^r \underline{w}^{r*} \qquad (4.1)$$

where

$$(\underline{w}^r)^T = (0, \ldots 0, w^r_{r+1}, \ldots w^r_N)$$

$\mathbf{w}^r$ is chosen so that elements r+2 to N of both row r and column r of the matrix become zero. The transformation also modifies all of rows r+1 to N and columns r+1 to N. The column is zeroed by

the premultiplication by P^r and the row by the postmultiplication. The achievement of one of these guarantees the other due to the symmetry of H. Consider the former requirement, i.e. the arrangement of $\mathbf{w}^r$ to zero the r'th column of P^rH, which we denote by $\mathbf{x}$. Partition $\mathbf{x}$ and $\mathbf{w}^r$ as follows :

$$\underline{x}^T = \left(\hat{\underline{x}}^T , x_{r+1} , \underline{y}^T \right)$$
$$\left(\underline{w}^r\right)^T = \left(\underline{0} , w^r_{r+1} , \underline{u}^T \right) \qquad (4.2)$$

Then
$$\rho^r \underline{x} = \begin{pmatrix} \hat{\underline{x}} \\ x_{r+1} - 2z w^r_{r+1} \\ \underline{y} - 2z \underline{u} \end{pmatrix} \qquad (4.3)$$

where
$$z = w^{r*}_{r+1} x_{r+1} + \underline{u}^* \underline{y}$$

The bottom section of this is to be zeroed, so we require :

$$\underline{u} = \alpha \underline{y}$$
$$1 - 2\alpha z = 0 \qquad (4.4)$$

Unitarity of the transformation requires :

$$\underline{w}^{r*} \underline{w}^r = 1$$

and hence
$$|\alpha^2| \underline{y}^* \underline{y} + |w^r_{r+1}|^2 = 1 \qquad (4.5)$$

Setting $\mathbf{w}^r_{r+1}=\alpha\mathbf{v}^r_{r+1}$, and eliminating α from (4.4) and (4.5), gives a quadratic equation for $\mathbf{v}^r_{r+1}$. The final result is :

$$w^r_{r+1} = \alpha\left(x_{r+1} \pm s\right) \qquad (4.6)$$

where $$\alpha = \frac{1}{\sqrt{2}}\left(s^2 + x_{r+1}s\right)^{-1/2}$$

and $$s = \left(x^2_{r+1} + \underline{y}^*\underline{y}\right)^{1/2}$$

The algorithm is found to be more stable if the sign of s is chosen to be the same as that of $\mathbf{x}_{r+1}$. Above its r+1'th element $\mathbf{w}$ is zero as required, and below it is proportional to the corresponding section of $\mathbf{x}$, as can be seen from (4.2) and the relation $\mathbf{u}=\alpha\mathbf{y}$.

For completeness, we also describe how the lowest eigenvalues of the tridiagonal matrix are found using Sturm sequences. In practice this is handled by a library subroutine, for example from the NAG library. Let T_r denote the r x r submatrix of T, and I_r the identity of the same order; then define the polynomial $P_r(\lambda)=\det(T_r-\lambda I_r)$, for some number λ. The sequence of all $P_r(\lambda)$'s for r=0,...N is called a Sturm sequence (see e.g. Golub & van Loan, 1983). The number of occurrences in this sequence of adjacent numbers with the same sign, denoted by $s(\lambda)$, can be shown to be equal to the number of eigenvalues of T which exceed λ. Thus an interval $[\lambda_1,\lambda_2]$ containing only one eigenvalue can be identified by the property that $s(\lambda_1)=k$ and $s(\lambda_2)=k+1$ for some $k < N$. Once such an interval has been found the eigenvalue can be "hunted

down" by trapping it in successively smaller and smaller bounds - the method of bisection. Each step consists of evaluating $s((\lambda_1+\lambda_2)/2)$ and replacing either λ_1 or λ_2 by their midpoint, depending on whether the result is k or k+1 respectively. In other words half the interval is discarded each time. The accuracy of the method can be very high, depending on the user's choice of stopping criterion.

4.2. Lanczos and fast Lanczos algorithms

The Lanczos tridiagonalising algorithm was conceived as long ago as 1950 (Lanczos 1950), but fell under a cloud for a long time because of its sensitivity to roundoff and the emergence of reliable "black box" methods such as those of Householder and Jacobi.

The Lanczos method was resurrected by Paige (1970), and has since proved to be excellent for computing the extremal eigenvalues and eigenvectors of symmetric matrices which are too large for transformational algorithms such as Householder to be feasible. It is also very attractive for sparse matrices due to lack of "fill-in", and has found important applications in lattice gauge theory (Barbour et al., 1985). The algorithm is eminently suitable for large electronic structure calculations because it is **recursive** and can be stopped after as few as $\sqrt{N}$ steps (Kahan & Parlett, 1976). The lowest eigenvalues (the ones we require) and

the highest are the first to emerge as those of the intermediate tridiagonal matrices. They can then be found by Sturm sequences as described at the end of section 4.1.

Unfortunately the algorithm is somewhat temperamental, in that there are no definite criteria for deciding when to stop the recursion. Its performance after a given number of steps depends on factors like the initial vector (see below), the spread of the desired eigenvalues and (especially) the arithmetic precision being used. But this disadvantage - the need for careful implementation - is significantly outweighed by the benefits of early termination, intrinsic speed (of order N^2) and economy of computer storage.

We now outline the algorithm. The given complex Hermitian matrix H and the (real) tridiagonal matrix T are related by :

$$HQ = QT \tag{4.7}$$

where $Q=(\mathbf{q}_1,...\mathbf{q}_n)$ is a N x N complex matrix composed of orthonormal columns, called the Lanczos vectors. Equation (4.7) is equivalent to a unitary transformation $T=Q^{+}HQ$, so no physical information is lost in going from H to T. Denote the elements of T as follows :

$$T = \begin{pmatrix} \alpha_1 & \beta_1 & & & 0 \\ \beta_1 & \alpha_2 & \ddots & & \\ & \ddots & \ddots & \ddots & \\ & & \ddots & \ddots & \beta_{N-1} \\ 0 & & & \beta_{N-1} & \alpha_N \end{pmatrix} \tag{4.8}$$

Then by matching the columns of the matrix products on each side of (4.7), it is straightforward to derive the Lanczos equations :

$$
\begin{aligned}
H q_1 &= \alpha_1 q_1 + \beta_1 q_2 \\
H q_i &= \beta_{i-1} q_{i-1} + \alpha_i q_i + \beta_i q_{i+1} \qquad (i = 2, .. N-1) \\
&\vdots \\
H q_N &= \beta_{N-1} q_{N-1} + \alpha_N q_N
\end{aligned}
\tag{4.9}
$$

The α's and β's are found recursively, starting from an (arbitrary) initial Lanczos vector $\mathbf{q}_1$. Usually $\mathbf{q}_1$=(1,0,0,...0) is an adequate choice. The α and β formulae are :

$$
\begin{aligned}
\alpha_i &= q_i^{\dagger} H q_i \\
\beta_i &= \| \beta_i q_{i+1} \| = \| H q_i - \beta_{i-1} q_{i-1} - \alpha_i q_i \|
\end{aligned}
\tag{4.10}
$$

where || || denotes the standard norm, the scalar product of the enclosed vector with itself. The next Lanczos vector is obtained by normalising $\beta_i \mathbf{q}_{i+1}$. It is clear from (4.10) that T will be real.

The algorithm may be written in a very economical form (Golub & van Loan, 1983). This is listed in (4.11) below.

This version only requires the storage of three N-vectors, namely **q**,**t** and **x**. Furthermore the costly multiplication by H is only performed once per cycle.

```
input q_1 ; β_1 = 0 ; x = 0
for j = 1 to k ( < N ) do
    if j ≠ 1 then { t = q_j ; q_j = x/β_{j-1} ; x = -β_{j-1} t }
  x = Hq + x
  α_j = q^+ x                                          (4.11)
  x = x - α_j q_j
  β_j = ||x||
next j
end
```

In exact arithmetic β_N will be zero, but this is impossible for N >10 or so in finite precision because the orthogonality of the **q**'s is destroyed by roundoff after a few recursions. It is remarkable that the accuracy of T's eigenvalues is not affected as a result. This is because the two sides of the recurrence relation (4.9) are still equal to within a single rounding error, regardless of the nonorthogonality of the $\mathbf{q}_i$; the important requirement in order for (4.9) to hold is in fact linear independence of the $\mathbf{q}_i$. This is discussed by Haydock (1980) in the context of recursive solution of Schrödinger equations, and by Parlett (1980).

When linear dependence starts to occur among the Lanczos vectors, copies of previous eigenvalues are generated due to repetition of the vector space spanned by earlier **q**'s. These copies are called 'ghosts'. When (or sometimes before) linear independence is completely lost, one gets spurious eigenvalues as well because nonorthogonality perturbations to the vector space are no

longer outweighed by the introduction of a new independent Lanczos vector. For large matrices, the emergence of both ghosts and spurious eigenvalues occurs fairly quickly, perhaps after 30 or so steps, as my results in chapter 5 demonstrate.

For large matrix problems the Lanczos algorithm's crowning advantage is the highly economical memory requirement. Firstly it can be seen from (4.10) that only two Lanczos vectors, $\mathbf{q}_i$ and $\mathbf{q}_{i-1}$, need be retained at any one time; and if the algorithm is coded as in (4.11), then only one further vector of length N is required. However if eigenvectors are desired (with a view to self-consistency) then older $\mathbf{q}$'s will still need to be kept in secondary store since the eigenvectors of H are obtained from those of T_j by multiplication by the N x j matrix $(\mathbf{q}_1,...\mathbf{q}_j)$ where j is the number of Lanczos steps actually performed. Secondly, in (4.10) the large matrix H only appears in the matrix-vector product $H\mathbf{q}$. Thus the matrix does not need to be stored explicitly — we only need to store its constituent information in a form suitable for multiplying a vector. This latter observation leads us to a major improvement to the Lanczos method as applied to electronic structure (with local potentials), which speeds it up from N^2 to NlogN. Its originator is unknown to me though it has been mentioned in passing in the context of the new molecular-dynamics techniques (footnote of Car & Parrinello, 1985 ; Allan & Teter, 1987). The key to it is the fact that the N x N matrix H has an information content of only N, having been constructed with respect to a basis of N plane waves $\{\mathbf{G}\}$. A nonlocal potential has an information content of order N(N+1)/2,

due to the distinct combinations of the ℓ quantum number with each pair of **G**'s, and so the following is not applicable (also see section 5.2). The local H may be simulated by a vector of length N. To achieve this we divide it into its two parts, the kinetic energy (which is diagonal) and the potential. In reciprocal space the product **Hq** is then :

$$\left(\underline{k}+\underline{G}\right)^2 q(\underline{G}) + \sum_{\underline{G}'} V(\underline{G}-\underline{G}')\, q(\underline{G}) \qquad (4.12)$$

Clearly the second term is a convolution, equivalent to the Fourier transform of the real space product V(r)q(r). If we do this product in real space and transform back, then the **Hq** operation (and hence the whole Lanczos algorithm) consists only of vector-vector multiplications and Fourier transforms. The Fourier transforms are the slower of the two and determine the overall timing. If the Fast Fourier Transform (FFT) is employed the timing scales like NlogN, which is a significant improvement on N^2 when N is of order 10^3 or more. The savings in memory demand and ease of programming are also considerable, especially if FFT routines already exist (for example in a library). The Lanczos method with the Fourier transform speed-up will hereafter be referred to as "fast Lanczos". Figure 4.1 shows a flowchart for the method, which should be read in conjunction with (4.10). The potential is input (or specified) in Fourier space and transformed to V(r) once only. Thereafter two FFT's are done on each Lanczos step. Using a serial computer to implement this algorithm for N up to 180, I confirm the NlogN variation of CPU time. Because a serial FFT is

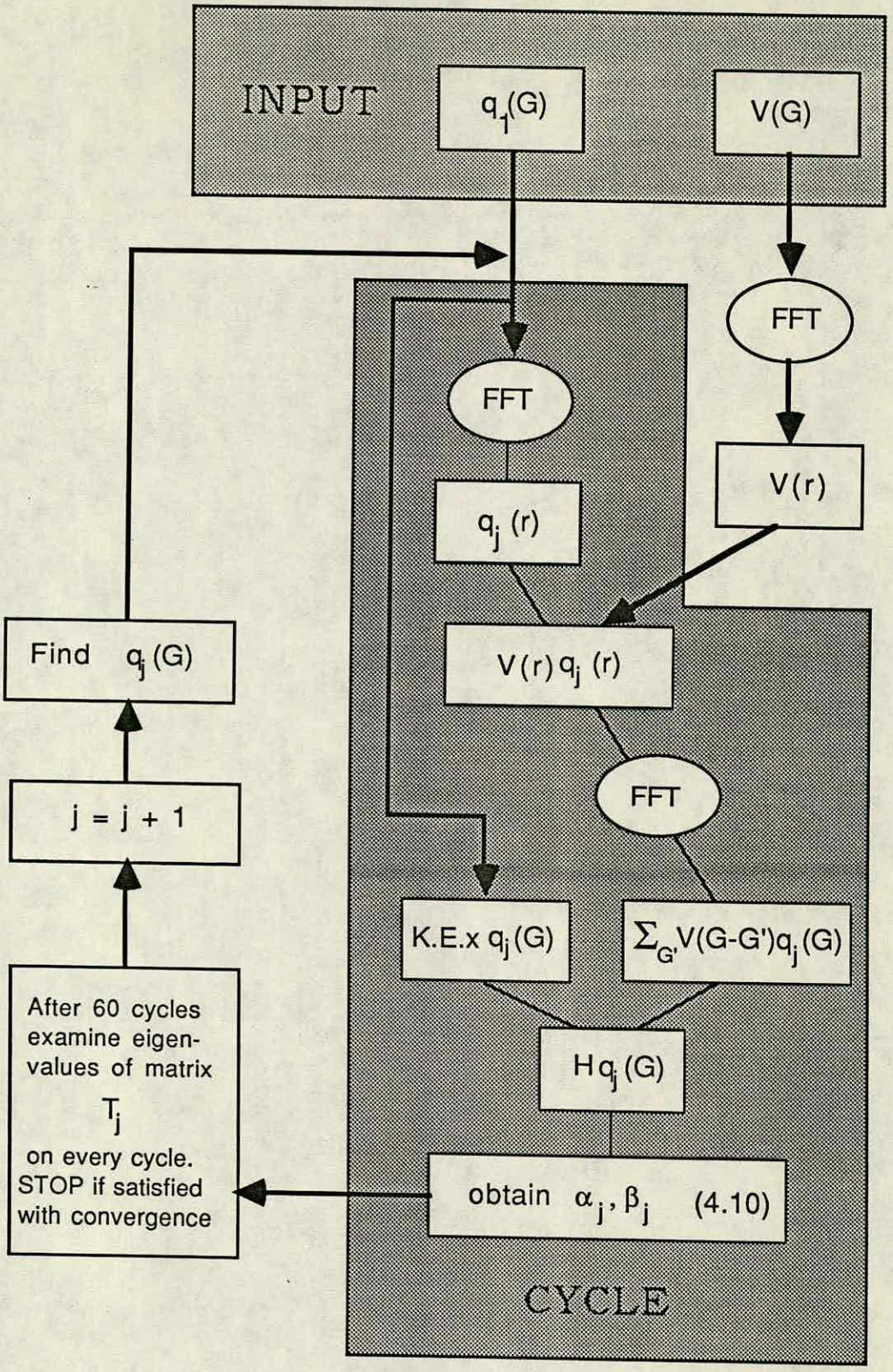

Figure 4.1. Flowchart for the fast Lanczos algorithm.

comparatively expensive for a large grid like the one of 16^3 which I employ, the times I observe are even slower than the Householder algorithm on the same machine. For N=64 on an Amdahl 470 computer, the fast Lanczos (inserted into the Schlüter code) takes 150 seconds while the old Householder version takes 9 seconds. However the fast Lanczos would overtake Householder at large N, due to its scaling like roughly $N\sqrt{N}\log N$ against Householder's N^3. The former figure assumes the maximum number of Lanczos steps needed to be of order $\sqrt{N}$ as mentioned earlier, although this upper bound is rather optimistic for large N. In any case, the fast Lanczos algorithm really comes into its own on a parallel computer, as we shall see in the next chapter.

5. PARALLEL IMPLEMENTATION

5.1 The ICL DAP

The DAP (Distributed Array Processor) was manufactured by International Computers Limited (ICL) from 1980 onwards. It is peripheral to a standard ICL mainframe like the 2900 series machine at Edinburgh, and therefore does not require its own operating system. It can even serve as extra memory for the mainframe when not in use as a processor. Enhanced versions of the DAP, incorporating up to date technology in the form of VLSI are now being manufactured by a new company, Active Memory Technology.

The DAP has a simple architecture, classified as SIMD (single instruction, multiple data), since the same instruction is simultaneously executed by all the constituent processors on their stored data. Examples of other machines with this architecture are the GEC GRID and the Connection Machine (Hillis, 1985). The other, more general, category of parallel architecture is MIMD (multiple instruction, multiple data) — for example, an array of independently programmable transputers — but this is harder to utilise effectively at present and would represent overkill for a matrix-type calculation like the fast Lanczos algorithm.

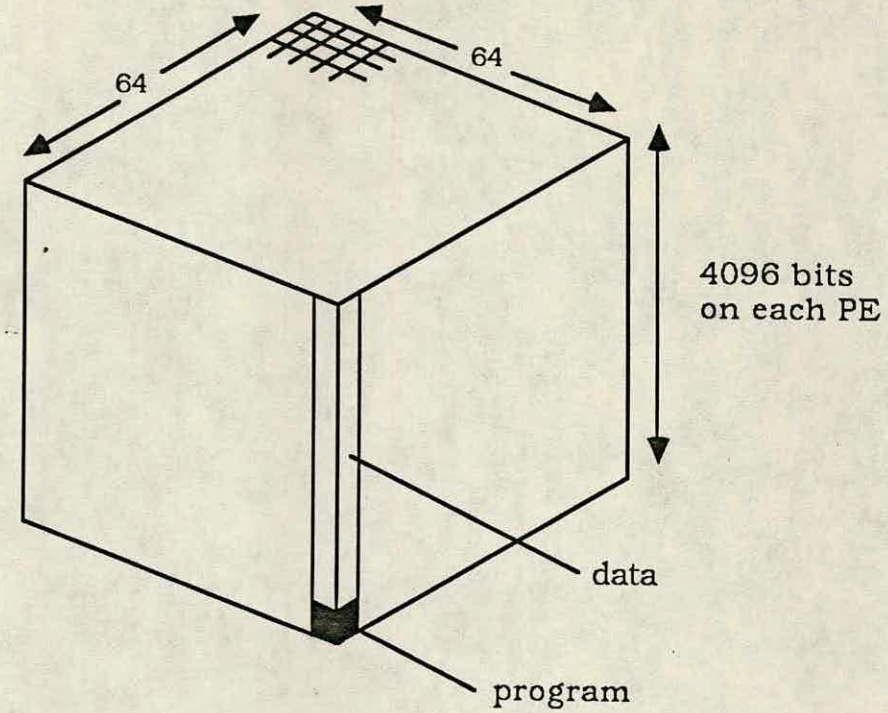

Figure 5.1. The ICL DAP

The DAP is a 64 x 64 array of simple processing elements (PE's), each consisting of 3 1-bit registers and an adder, plus 4K of RAM. This local store on each PE gives the machine a quasi-3-dimensional form (see Figure 5.1). The total memory is therefore 2 Mbytes. The usual data structures are 64 x 64 matrices, 64-vectors and scalars; an array of 4096 elements can also be handled as a vector. To exploit these architectural features, the DAP is programmed in an extension of FORTRAN called DAPFORTRAN. For example, two 64 x 64 matrices can be added together by means of a single DAPFORTRAN instruction :

$$C = A + B$$

where a serial FORTRAN program would require 2 loops :

```
      DO 100 I = 1,64
      DO 100 J = 1,64
      C(I,J) = A(I,J) + B(I,J)
100   CONTINUE
```

As well as brute parallelism, the DAP architecture has the more elegant attribute of connectivity. Every PE is connected to its four nearest neighbours (edge processors have wrap-around connections to the opposite edge) and can pass data to them. Furthermore, each PE has limited local control in the form of an activity control bit, which masks the data stored in that PE when activated. Accordingly DAPFORTRAN is capable of some very powerful constructions, involving combinations of shifting, summing and logical masking of data arrays. The fast Lanczos application exploits these aspects of the DAP's power only insofar as it performs 16 MERGE's and 2 SUM's per iteration. The function MERGE(A,B,L) takes as input two 64 x 64 matrices A,B and a logical mask L and returns a matrix containing elements of A wherever L has true elements and of B wherever L is false. In our case A is (part of) the convolution $\Sigma_{G'}V(G-G')\mathbf{q}(G)$, produced by an FFT, and B is zero. The mask, which is set up in the host machine, corresponds to the chosen basis of N reciprocal lattice vectors, which is a subset of the 32768 points on the (32^3) FFT grid. The MERGE thus zeroes the elements of the convolution corresponding to plane waves outside the basis, leaving a set of N nonzero elements which can safely be combined with the kinetic energy in the next step of the algorithm. In practice 16 MERGE's are needed because A is a vector with 32768 complex elements and therefore must be represented on the DAP by 16 64 x 64 matrices, 8 for the

real parts and 8 for the imaginary parts. The basis mask L occupies 8 matrices, being the same for both real and imaginary parts.

The SUM function is self-explanatory and is used in the calculation of the two scalars, α and β (see eqn. (4.10)). The former is given by the sum of the vector-vector multiplication $\mathbf{q}^{+}\mathbf{w}$ and the latter by a vector norm, i.e. the square root of a sum.

Those readers who are not satisfied by the selective discussion given above will find the main DAP program, with annotation, in the Appendix.

As the DAP can only be accessed through the mainframe host, a DAP program has to be written as an entry subroutine which is combined with the calling host program at the execution stage. Data is passed between host and DAP via COMMON blocks, and conversion statements are also necessary because data is stored in a different format in the DAP. Thus, although the DAP appears to the mainframe as a piece of its own store, the overheads for data transfer are not inconsiderable.

5.2. Implementation of the fast Lanczos algorithm

This section outlines the specific features and problems of the implementation of the pseudopotential code with fast Lanczos on the DAP. Since most of these are related to the Fast Fourier Transform (FFT) we discuss this first.

The discrete 1-dimensional Fourier transform of N_F data points $x_0, x_1, \ldots x_{N_F-1}$ (the subscript is to avoid confusion with basis size N) is given by :

$$X(k) = \sum_{n=0}^{N_F-1} x_n W^{nk} \qquad (5.1)$$

where $$W = \exp(-2\pi i / N_F)$$

The superscript nk on W is an exponent. The FFT gains speed by decomposing N_F into m factors (preferably powers of 2) and reformulating the 1-dimensional transform as a quasi-m-dimensional transform. It should be of interest to the reader that this key idea was first proposed by Danielson and Lanczos (1942), the latter being more well known for his matrix algorithm!

Considering the case m=2, the single row of data points (say 64) becomes a 2-dimensional array (perhaps 16 x 4), each row of which is transformed separately. The result has to be reshuffled into the correct order via a "butterfly" mapping (see e.g. Brigham, 1973). The process lends itself well to parallelisation because

(in our example) the 16 rows of 4 points are independent and can be processed simultaneously. A 3-dimensional transform, as we require for the fast Lanczos, is equivalent to three nested 1-dimensional transforms. It is natural to use a 3-dimensional grid with dimensions corresponding to 3 factors of N_F. These dimensions may in theory be any integers (not necessarily equal), but the programming is easier, and the program runs much more efficiently, if they are all the same power of 2. This is especially important in the case of the DAP, whose architecture virtually demands the use of powers of 2 (e.g. a 65 x 65 matrix is twice as expensive to store as one of 64 x 64). The DAP's inflexibility in this respect is worthy of comment. The 2-dimensional FFT in the DAP subroutine library uses a 64 x 64 grid. The prior existence of this routine greatly facilitates the coding of a 3-dimensional routine on the DAP (Brass & Pawley, 1986), as the 3-d FFT is equivalent to a 1-d transform applied to the results of a 2-d FFT. I use 3-d subroutines written in this way by Brass (32^3), and by Sheard (16^3).

For the ranges of reciprocal lattice vectors encountered in pseudopotential calculations, the FFT grid dimension should be either 16 or 32. The memory requirement (total number of grid points) scales like the cube of the dimension, so that a 32^3 lattice requires 8 times as much storage as one of 16^3. The fast Lanczos subroutine with a 16^3 FFT will comfortably fit into the DAP's 2 Mbyte memory in double precision (REAL*8) arithmetic. However, the 32^3 FFT will fit only if the precision is halved to REAL*4. As discussed in section 4.2, the loss of linear independ-

ence due to roundoff produces a concomitant reduction in algorithm performance, as shown by a comparison of Figure 5.2 (16^3, double precision) and Figure 5.3 (32^3, single precision). A different matrix is being solved in each case, but both are of order 300 or so and Lanczos is stopped after 64 steps (the most we should need). These plots suffice to show both the accuracy and the rate of convergence of the eigenvalues. In the case of single precision on the 32^3 grid, it is clear that the higher eigenvalues converge much more slowly.

We remark here that Figures 5.2 and 5.3 also show the spurious eigenvalues, as isolated dots lying between the horizontal "rows". These are removed in future work by calculating the eigenvalues on the last 3 or 4 Lanczos steps, and discarding from the last set those which differ by more than some small quantity (5×10^{-4} eV was found to be effective) from all the numbers in the preceding 2 or 3 sets. Ghosts are also removed by applying a similar criterion in reverse manner (i.e. adjacent numbers within 5×10^{-4} eV) to the list of eigenvalues from the last step only.

While testing these filters I found that the rate of convergence of eigenvalues was slightly improved by adding a quantity like 10 or 20 Ry to the kinetic energy vector, thus giving the low eigenvalues (previously of order 1 Ry) a relatively large modulus. The same quantity is, of course, subtracted from the eigenvalues at the end of the calculation. Returning to the question of FFT grid size, it would be desirable to stick to 16^3 in order to use double precision arithmetic. Unfortunately, however,

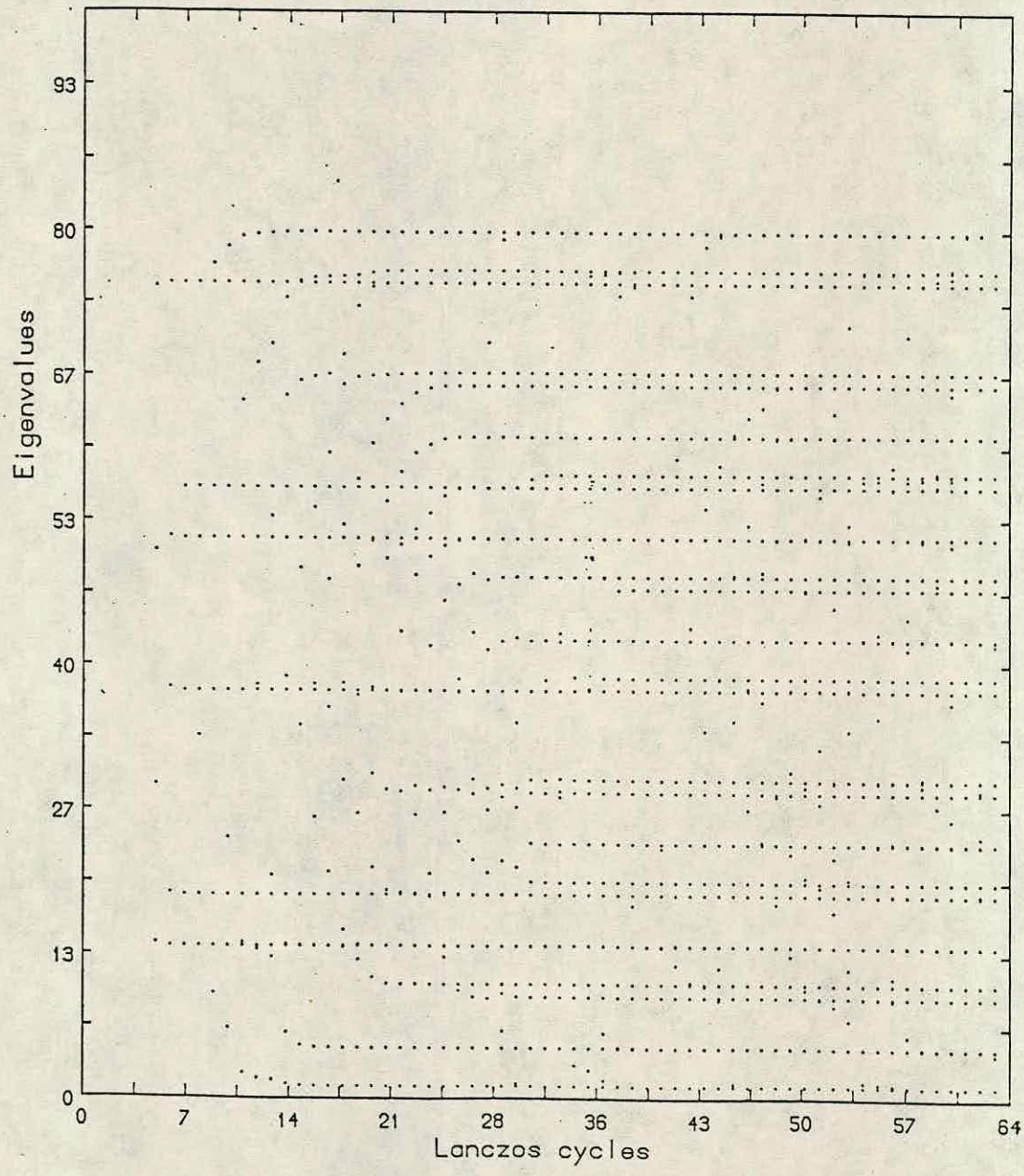

Figure 5.2. Emergence of eigenvalues: 16^3 FFT, REAL*8 arithmetic

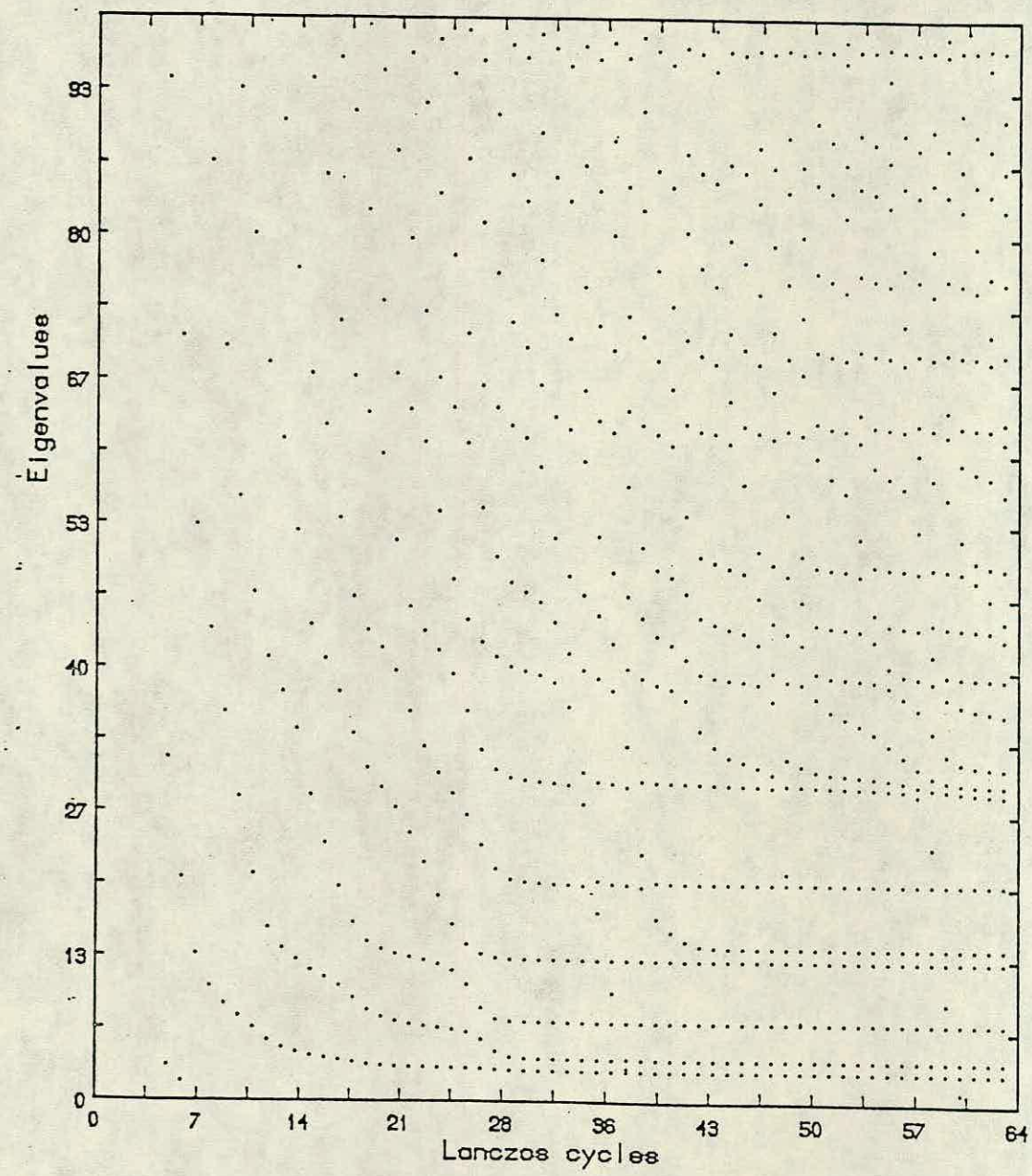

Figure 5.3. Emergence of eigenvalues: 32^3 FFT, REAL*4 arithmetic

this introduces limitations on the available reciprocal lattice vectors, as there are then only 16 grid points in each direction. Thus one is limited to indices running from -7 to 7. This is effectively a 15^3 grid, but the addition of only one of either -8 or 8 would make the whole matrix non-Hermitian, and cause the Lanczos algorithm to break down, as Figure 5.4 illustrates. This shows plots, with both 16^3 and 32^3 grids, of part of the band-structure of $(GaAs)_4(AlAs)_4$, a layered system in which short wavelength Fourier components should be important; for example the (008) matrix element is 0.0337, just one order of magnitude smaller than the long wavelength elements clustered around the origin. The 16^3 grid omits either the (008) or the equivalent (008) element (as well as all higher elements) and the resulting change is seen from Figure 5.4 to be significant.

Since it is hoped to study systems with periods even longer than 4 layers of each material, it is evident that the 16^3 FFT grid is not sufficient. This is unfortunate as the 32^3 grid, even with precision reduced to REAL*4, leaves no room in the DAP for reconstructing Hamiltonian eigenvectors from those of the matrix T_j. This is because all the Lanczos vectors cannot be stored. If the algorithm is stopped at the usual point, after 64 steps, the 64 Lanczos vectors (each with 32^3 elements) would occupy 8 Mbytes, four times the DAP's capacity. The Edinburgh system has a data transfer facility between DAP and disc filestore. In principle, this could be used to support REAL*8 arithmetic on a 32^3 grid, and possibly the reconstruction of eigenvectors. However, the following argument shows that this is not practical. The data

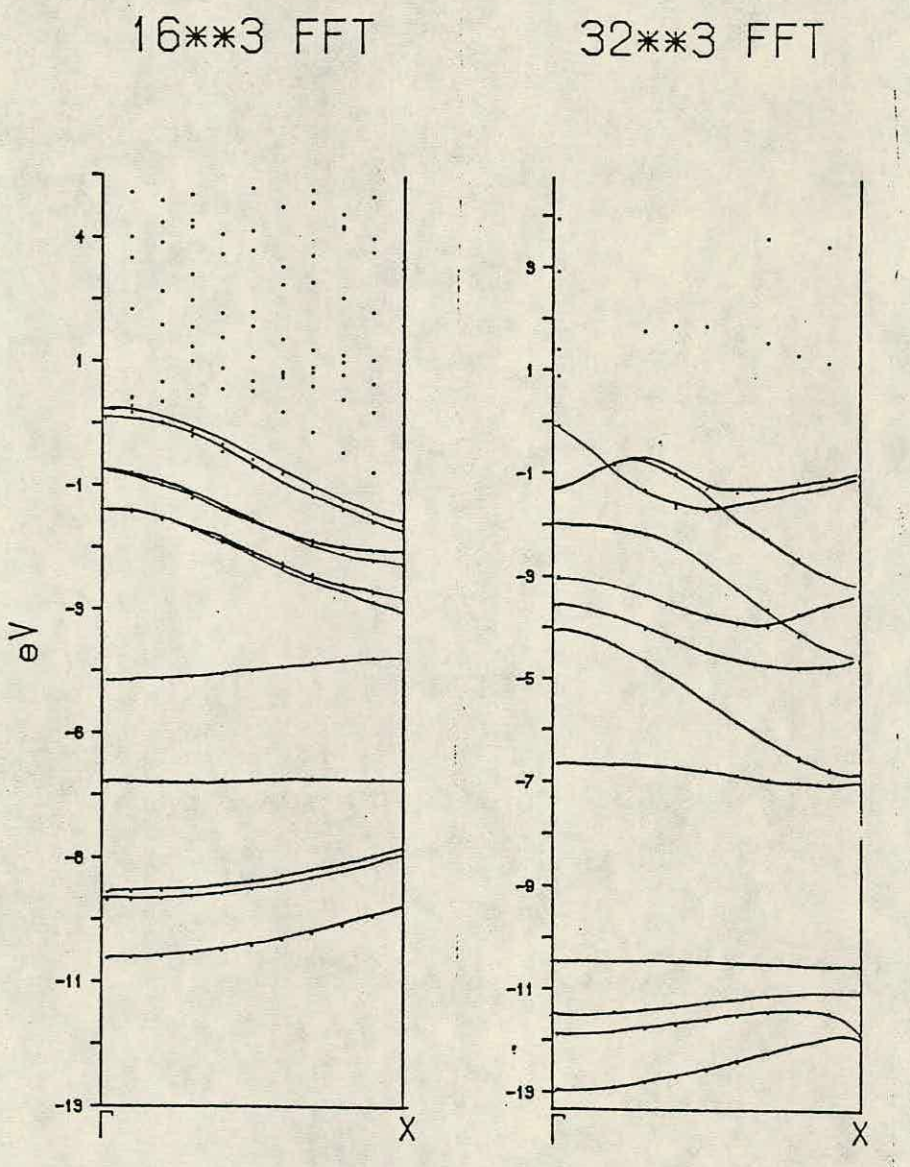

Figure 5.4. Γ-X bandstructures for $(GaAs)_4(AlAs)_4$

transfer rate between DAP and disc is in practice somewhat greater than 100 kbytes per second - say 20 kwords per second maximum in REAL*8 precision (one word has 8 bytes). In this precision, the DAP operates at roughly 5 Mflops. Hence, for acceptable overheads on the transfer, each word must be used in about 250 arithmetic operations. Unfortunately, the FFT algorithm is so effective that only of order $\ln N_F$ operations per word are required, and this is at least an order of magnitude too small.

We also note that, for very large or complex systems ($N >> 1000$), the algorithm will need to be continued somewhat beyond 64 steps to converge all the eigenvalues and also ensure that the eigenvectors and charge densities are sufficiently accurate for self-consistent calculations. This would increase the memory demands of the 32^3 grid even further. One way of ensuring that 64 steps is sufficient for any system might be to add selective orthogonalisation to the algorithm (Parlett and Scott, 1979); this orthogonalises the current $\mathbf{q}_i$ to all its predecessors whenever cumulative loss of orthogonality rises above a certain level. This does require storage of the previous $\mathbf{q}$'s, but they will be stored anyway if one is going on to obtain the eigenvectors.

To summarise, in view of the inadequacy of a 16^3 FFT for long-period heterostructures, we use 32^3 for all the calculations reported in the next chapter, although this involves sacrificing both self-consistency and double precision arithmetic. Another option might have been to write my own FFT routine for a 27^3

grid, which would have allowed an increase in precision to REAL*5 or REAL*6 (any word length from 3 to 8 is allowed on the DAP, although nonstandard lengths would be difficult to interface to the host), or the use of REAL*4 with selfconsistency. This was not feasible in the available time, however.

We also make a third sacrifice by eschewing nonlocality and using only local pseudopotentials. This is not due to any limitations of the DAP itself, but to a more general computational problem, namely that the matrix elements of the Hamiltonian are nonseparable when a nonlocal potential like that of BHS is used. In other words, the elements $\langle \mathbf{q}|V|\mathbf{q}'\rangle$ are not expressible in the form $\Sigma_t f_t(q) g_t(q')$, $t \ll N$. This is because the nonlocality is actually limited to angular coordinates, and the potential is still local in the radial coordinate. The term "semilocal" (SL) has been coined to describe this state of affairs. The matrix element between **q=k+G and q'=k+G'** is given by :

$$\langle \underline{q} | V_{SL} | \underline{q}' \rangle = \sum_{l} 4\pi(2l+1) P_l(\cos\theta_{qq'}) \times \int_0^\infty r^2 j_l(qr) j_l(q'r) \delta V_l(r) d^3r \qquad (5.2)$$

where j_l is a spherical Bessel function, P_l is a Legendre polynomial and $\theta_{qq'}$ is the angle between the two vectors. The nonlocal correction $\delta V_l(r)$ goes to zero just beyond the

pseudopotential core radius r_c, as it must by the definition of a norm-conserving potential. In (5.2) q and q' appear in the same integral and so one has to perform a total of MN(N+1)/2 separate integrals, where M is the number of **k** points chosen and N is the number of plane waves **G**. With typical values for hetero-structure systems like M ~ 20 and N ~ 1000, the number of integrals would be 10^7, which is prohibitive. With the Schlüter code on a NAS 7000, the setting up of such a matrix would take a time of order 1 hour. More important from our point of view is the fact that the nonseparable potential defined by (5.2) cannot be Fourier transformed to a real space function V(r), and so the fast Lanczos algorithm as outlined in Figure 4.1 cannot be used. To put it another way, the nonlocal (e.g. BHS) Hamiltonian contains too much information to be representable by a vector (see section 4.2).

A way of constructing a separable nonlocal pseudopotential has recently been proposed (Kleinman and Bylander, 1982). Since the pseudopotential is arbitrary, V_{SL} may be replaced by a fully nonlocal form V_{NL}, for which the matrix element is :

$$\langle \underline{q}|V_{NL}|\underline{q}'\rangle = \sum_{l} 4\pi(2l+1)\, P_l(\cos\theta_{qq'}) \times$$

$$\ldots \frac{\int_0^\infty r^2 j_l(qr)\,\phi_l(r)\,\delta V_l\, d^3r \int_0^\infty r^2 j_l(q'r)\,\phi_l(r)\,\delta V_l\, d^3r}{\int_0^\infty r^2 [\phi_l(r)]^2\,\delta V_l(r)\, d^3r} \qquad (5.3)$$

where $\phi_l(r)$ is the atomic radial pseudowavefunction used in the BHS construction (see Section 3.2). q and q' now occur in different

integrals (of the same form) and so only MN integrals need to be evaluated altogether. V_{NL} can also be transformed to real space, so the fast Lanczos algorithm can be used. Unfortunately the method presented by Kleinman & Bylander for constructing a suitable V_{NL} involves an enormous amount of trial and error, and in their paper they only applied it to tungsten. It is not feasible for me to repeat this work for 3 further elements (Ga, Al and As) and so I am limited to using local pseudopotentials. The potentials I actually use are described in the next chapter.

Using local potentials, the DAP implementation of the fast Lanczos algorithm takes 0.5 sec per Lanczos step for all N up to 32768. Most of this time is spent doing FFT's. Stopping after 64 steps (as I do) gives a timing of about 30 sec per **k**-point, for any size of Hamiltonian. This independence of the size of basis set is a reflection of the lack of flexibility in DAP programming, but it is also very advantageous when compared with, say, the N^3 dependence of the serial Householder algorithm, and more than justifies the effort of using the DAP.

We close this chapter by mentioning the problem of degeneracy. The Lanczos algorithm does not explicitly give degenerate eigenvalues, unlike Householder. Numerous multiple eigenvalues do appear in the Lanczos output but these include a lot of 'ghosts' due to imperfections inherent in the algorithm (as discussed in section 4.2), as well as true degeneracies. It is important that the program knows which eigenvalues are degenerate, so that it will find a separate eigenvector corresp-

onding to each degenerate eigenvalue. (Incidentally it is necessary to add small random numbers of order 10^{-5} Ry to the eigenvalues in order to lift each degeneracy sufficiently for different eigenvectors to emerge.) The necessary information could be deduced from group theoretic considerations, but this would be very tedious for complex systems, and increases the amount of input data required by a calculation. A more attractive option, and one which is easily programmable, is to obtain the degeneracies directly from inspection of the Householder solution of a small submatrix (say 50 x 50) of the full Hamiltonian, chosen to include the largest elements on the main diagonal. If human involvement is to be avoided, the size of submatrix has to be adequate for the computer to be able to pick up all the degeneracies, in the form of sets of nearly coincident energies; an appropriate size would need to be established by trial before embarking on serious work.

6. APPLICATION TO SUPERLATTICES

6.1. Low dimensional structures

When substantially modified in just one of the three dimensions, materials can exhibit some interesting and technologically important properties. The best example of this is the semiconductor superlattice, consisting of alternating thin layers of two (or more) materials. This was first proposed by Esaki and Tsu (1970) and then grown by the new epitaxial techniques, in which the layers are built up with great precision (thanks to self-smoothing), by firing high temperature beams of the appropriate atoms at a substrate under clean high-vacuum conditions. In the material with the smaller energy gap the electrons are in a quantum well and behave as if limited to two dimensions, an example of a quantum size effect (see Figure 6.1).

If b is the thickness of one layer, typically 10-100 Å, then the energy quantum in the z direction (perpendicular to the layers) varies like $1/b^2$ and is much larger than the (infinitesimal) quanta in the x and y directions. Thus the quasi-continuum (in real space) of an ordinary bulk solid is replaced in a superlattice by a system of separate 'minibands', or regions of allowed energies. If for the sake of argument we approximate the system by a series of infinite wells, the separation between the lowest two minibands will, according to elementary quantum mechanics,

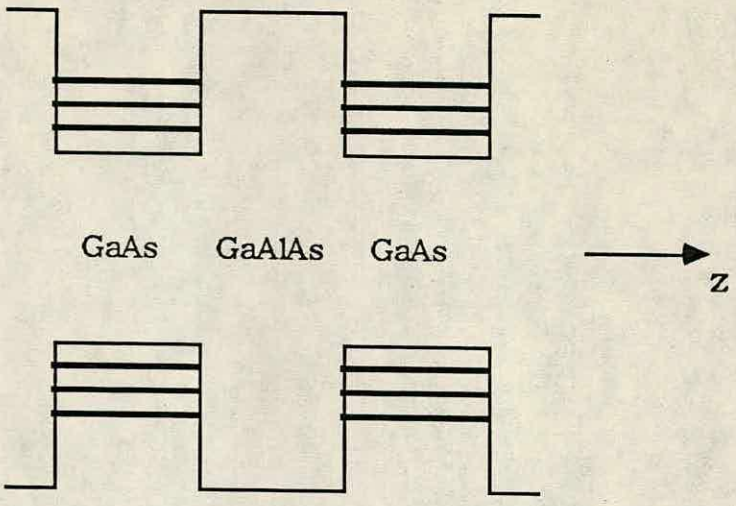

Figure 6.1. Quantum well formation in a semiconductor heterostructure

be given by :

$$\Delta E_{12} = \frac{k^2 \pi^2}{2 m_e b^2} \left(2^2 - 1^2\right) \qquad (6.1)$$

For b = 30Å (about 6 atomic spacings in GaAs) this is equivalent to 1500K, so electrons remain in the 1st miniband at reasonable temperatures. Within each miniband the electrons obey 2-dimensional dynamics, as they have the same k_z. Therefore the electron gas is effectively 2-dimensional in both an energetic and dynamic sense, notwithstanding the finite extent of the layer in a third dimension. The study of quantum well systems has yielded much important physics, the prime example being the quantum Hall effect.

Figure 6.1 shows a schematic view of a GaAs/$Ga_{1-x}Al_xAs$ superlattice, in which the GaAs has the smaller gap. This particular system is the most frequently studied to date because the very small (0.2%) lattice mismatch between the two constituents facilitates its growth, and its effective energy gap lies around the visible region of the electromagnetic spectrum, making it important for optical applications. The Al fraction x in the alloy has to be less than 0.4, otherwise the alloy gap at Γ would be indirect, due to the material being AlAs-like.

The real power of the superlattice concept lies in the tunability of the properties, especially the energy gap. The overall gap in reciprocal space is dependent on the layer thicknesses and can thus be varied between the two extrema set by the choice of materials. Decreasing the layer thickness increases the gap, and vice versa. Obviously the gap also depends on the constituent materials, and on the composition of any alloys that are present; for example the gap in $Ga_{1-x}Al_xAs$ increases with x. Other systems often studied include InAs/GaSb and SiGe/Si. The latter is interesting because the two constituents have lattice constants differing by 4.2% - the mismatch being completely accommodated by strain. This removal of the lattice matching requirement suggests that a vast number of different superlattices could be made, and calculations of the bandstructure and properties will play a vital role in advising which ones are really worth growing.

There is also another type of superlattice called the doping superlattice (to distinguish it from the compositional superlattice discussed above), which consists of only one material (Döhler, 1983). The heterogeneity is achieved by different doping i.e. n-type and p-type layers, with thin intrinsic layers in between to prevent interfaces acting as diodes. This type offers another way of tuning properties, through variation of the doping. The gap can even be tuned after construction, by applying potentials to the layers in such a way as to partially cancel the doping.

We now discuss the applications of superlattices, apart from new physics such as the quantum Hall effect. Superlattices are very useful in optoelectronics because of their tunable (and in the case of doping superlattices, externally controllable) optical properties. Devices manufactured or proposed include light detectors, modulators and optically bistable switches (Miller et al., 1984). Multiple quantum well lasers have also been made (Holonyak et al., 1980), by setting up a population inversion between the conduction band of the wide-gap material and that of the narrow-gap material (i.e. the top and bottom of each quantum well). As well as adjustability of the beam colour, MQW lasers enjoy several significant advantages over conventional semiconductor lasers, such as low power consumption and high current density (hence a stronger beam).

The second major application area is high speed digital circuits, incorporating the fastest transistor ever made, the HEMT

(High Electron Mobility Transistor). Japanese technologists have achieved switching speeds of 50 picoseconds at room temperature (Mimura et al., 1980). The very high mobility is achieved by modulated doping of a compositional superlattice such as GaAs/GaAlAs. This is done during growth by, for example, synchronising a Si beam with the Al so that only layers of GaAlAs (the large gap material) are n-doped. The extra conduction electrons fall to the lowest miniband in the well, where they can move freely without being scattered by the fixed donor ions as they would be in any uniformly doped system. Figure 6.2 shows how this spatial separation works. The scattering impurities are shown by dots.

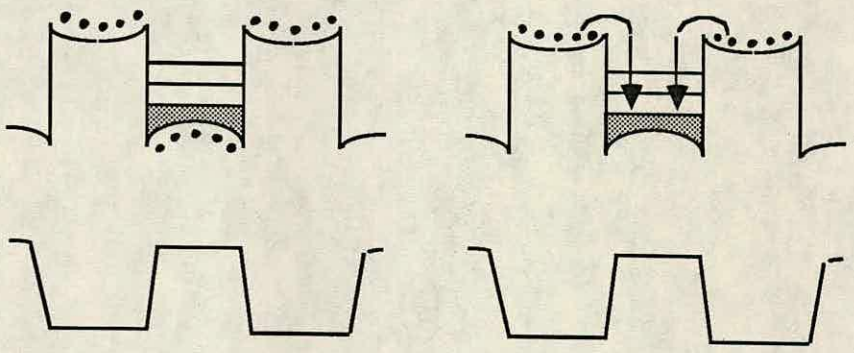

Figure 6.2 L : uniform doping. R : modulated doping.

Other projected applications of superlattices include solid state microwave generators at wavelengths below 1 mm (which do not exist as yet). In the future lies the tantalising prospect of 3-dimensional microelectronics, based on "lateral" heterostructures.

6.2. Review of superlattice calculations

The region at the junction of two semiconductors is theoretically complex. In an interface between differently doped versions of the same material, called a homojunction, the properties are determined primarily by the electric field due to band bending, and are well understood. In a heterojunction however, the mismatches between the two sets of semiconductor parameters (especially the energy gaps and mobilities) have a profound effect on properties, as do many microscopic factors caused by the inhomogeneity. It is still very difficult to predict, or even measure experimentally, the band lineup. By this we mean the conduction band offset and the valence band offset at the interface. For device applications both offsets are of great importance and need to be known to meV accuracy. The experimentalists may achieve this first, given more powerful synchrotron radiation sources for photoemission studies (Bauer & Margaritondo, 1987). Theorists' best hope seems to lie with ab initio pseudopotential calculations rather than the competing "model" theories (e.g. Tersoff, 1984). This is because the latter invariably make uncontrolled assumptions, such as the introduction of a reference level for lining up bands. Features like band offsets and the relative position of conduction band minima are extremely sensitive to the potential used. On moving to a superlattice, namely a series of heterojunctions, the physics of the problem becomes even more complex, especially for thin layers (which exhibit the greatest departure from bulk behaviour). The band

offsets are expected to vary significantly with the superlattice period, and with other factors like interfacial strain (if present). A systematic ab initio framework is then of even greater importance as it has the capability to account for all properties. This even includes the crystal structure — an important issue for a system with two competing phases like $(GaAs)_1(AlAs)_1$. On the other hand an empirical approach or a model can only ever be partially successful.

Progress on the ab initio front will no doubt be encouraged by the recent important demonstration by van de Walle & Martin (1986) of the feasibility of calculating the band offsets at an interface (Si/Ge in their case) entirely within an ab initio framework. This direct link to device engineering should help ab initio workers to triumph over the proponents of empirical models and other "fixes".

Only in the last couple of years have ab initio pseudopotential workers been able to rise to the challenge presented by heterostructures. This is because of the large matrices which arise from the use of long unit cells (of order 10 atoms or more). The longer the cell, the shorter is the shortest wavevector in the z direction and hence the greater is the number of plane waves needing to be incorporated into the basis. Matrices of order 1000 or above make some form of supercomputer necessary for self-consistent calculations. Expensive coding techniques are also necessary for nonlocal potentials, as we saw in the previous chapter.

The state of the art at the time of writing (apart from Car-Parrinello type calculations) is probably the newly published work of Ciraci & Batra (1987). They used BHS pseudopotentials and a basis of 1200 plane waves for selfconsistent studies of $(GaAs)_4(AlAs)_4$ and Si_4Ge_4, and their charge density results are the first to demonstrate clearly the confinement of electrons to the quantum wells. Another recent selfconsistent ab initio calculation is that of Bylander & Kleinman (1986) for $(GaAs)_1(AlAs)_1$, the result of which is one of those displayed in Figure 6.5 (next section) for comparison with my results. This paper is hereafter referred to as BK.

Over the last ten years many selfconsistent **empirical** calculations have also been done, starting with the pioneering work of Pickett, Louie & Cohen (1978) for $(GaAs)_9(AlAs)_9$, using about 1100 plane waves (700 of them perturbatively) on an 18-atom unit cell. This work, hereafter denoted by PLC, is the source of my empirical potentials (see Figure 6.3, next section). The best empirical calculations on $(GaAs)_n(AlAs)_n$ to date appear to be those of Nakayama & Kamimura (1985) for n=1-8 and of Ferraz & Srivastava (1986) for n=1-9. Both use local pseudopotentials and X-α screening. The former used slightly modified PLC potentials, and adjusted α to simulate the correct gaps. For the n=2 superlattice, they demonstrated the folding of the bands along Γ-Z (see Fig. 6.10) and also investigated the 'character' of AlAs and GaAs contained in the bands. The latter used the bare potentials of Chelikowsky et al. (1981).

The empirical pseudopotential calculations of the Jaros group (e.g. Gell et al., 1986) represent the leading edge of a somewhat different approach, which seeks an alternative to selfconsistency and the attendant imperfections of the density-functional screening formalism. In this method the heterogeneity of the superlattice is treated as a perturbation on one of the constituents in the bulk state. For example, $(GaAs)_n(AlAs)_n$ can be regarded as GaAs perturbed by the substitution of half the Ga atoms by Al atoms. The basis functions of the system are bulk wavefunctions (of GaAs in our case), which are much more representative of the whole system than plane waves, leading to a small and easily soluble matrix. On the debit side one has the perennial problem of constructing a realistic empirical potential for use in a one-off calculation, and the methodology currently proposed is not particularly rigorous.

Several of the workers mentioned above will feature again at the end of the next section, for example with regard to Figure 6.12, which will show the energy gap against layer thickness from various calculations.

We observe that the general trend to date has apparently been to concentrate attention on $(GaAs)_n(AlAs)_n$, rather than on systems also incorporating the alloy $Al_xGa_{1-x}As$. There are probably two reasons for this. Firstly the former system is simpler, being equivalent to the special case x=1, and is proving to be of some technological interest in its own right. The work done on the combination of pure materials should supply a good foundation

for similar work on more sophisticated alloy systems. In addition, $(GaAs)_1(AlAs)_1$ has been the topic of some controversy since the X-ray observations of Kuan et al. (1985), which suggested that the monolayer superlattice is actually the equilibrium state that results from random growth sequences, instead of the random alloy $GaAlAs_2$ that one would naively expect. The careful calculations of BK provided conclusive theoretical confirmation of this interesting fact.

Of the authors mentioned above, only Ferraz & Srivastava, and Gell et al., have explored the $GaAs/Al_xGa_{1-x}As$ system to any extent. This system is certain to receive more attention in the future because of the greater range of properties accessible through variation of x, and its historical position (due to ease of growth) as the prototype for all other alloy systems.

For completeness, we end our short review by mentioning the envelope function approach, which is the preferred choice of those who are sceptical of the large-unit-cell large-matrix methods, and simply want to extract information about the states around the gap at the Brillouin zone edges, which contain most of the physics for practical applications. It involves expanding the actual wavefunctions on each side of the interface in (slowly varying) envelope functions, one for each band. On matching these envelope functions, a selfconsistent Schrodinger equation is obtained and can be solved iteratively. Systems studied with this method include a doping superlattice (Brand & Abram, 1983) and $GaAs/Al_xGa_{1-x}As$ (Hurkx & van Haeringen, 1985). However, there are uncertainties about the applicability of this approach.

6.3. Results

In this section we present the results of my work and set them in context. The empirical potentials I use were tabulated by PLC (Pickett, Louie & Cohen, 1978), who fitted both screened and unscreened potentials in momentum space to a formula with 4 parameters in such a way as to reproduce bulk bandstructures. Denoting wavevector (in atomic units) by q and the parameters by $b_1,...b_4$, the formula for V(q) in rydbergs is of the form :

$$V(q) = \frac{b_1(q^2 - b_2)}{\exp\left[b_3(q^2 - b_4)\right] + 1} \qquad (6.2)$$

Being limited to nonselfconsistent calculations, we choose the screened potentials, for which the parameters for the 3 elements of interest are listed in Table 6.1.

	Al	Ga	As
b_1	0.4489	10.2179	1.1321
b_2	1.8800	2.3846	2.6533
b_3	0.6500	0.5598	0.6825
b_4	-0.300	-6.4574	-1.2769

TABLE 6.1. PLC potential parameters

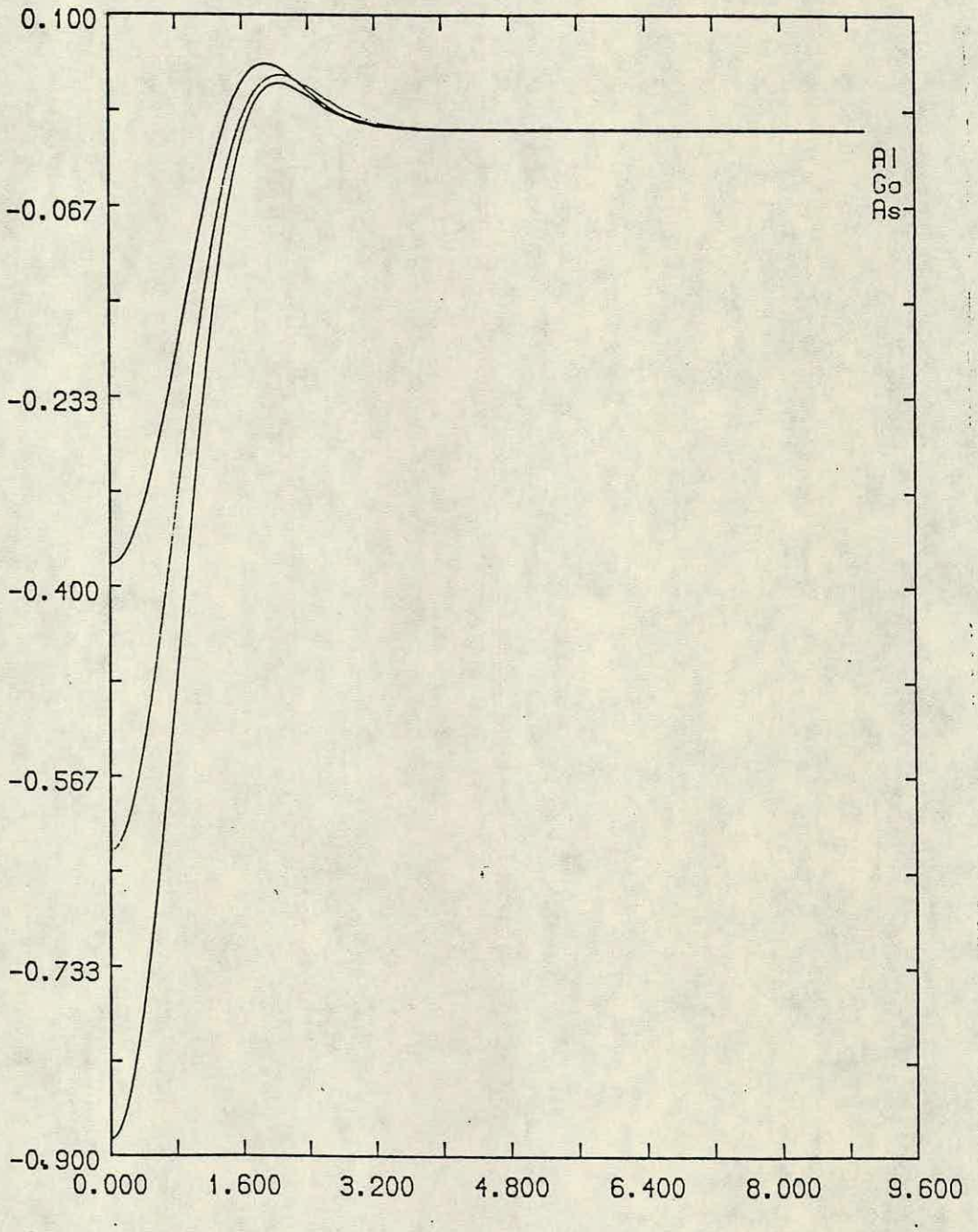

Figure 6.3. The screened empirical pseudopotentials parametrised by Pickett et al. (1978)

Note that the fitting has been performed for fcc wavevectors, the zincblende lattice (fcc with a 2-atom basis) being the most natural choice for the description of III-V compounds. The potentials are normalised to a unit cell volume of 152.9 a.u.^{3}. These three V(q) are depicted in Figure 6.3. They tend to zero as $q \rightarrow \infty$ and to $-2E_F/3$ as $q \rightarrow 0$. The well depth is seen to increase with atomic number, as expected. These potentials are stated to be inaccurate for small q, being only intended by PLC for use on the first iteration of a selfconsistent calculation.

We emulate BK by using a simple tetragonal unit cell, rather than the more usual fcc cell. I believe Caruthers & Lin-Chung (1978) were the first to use a tetragonal cell in this context. The top half of Figure 6.4 depicts the lattice vectors in both real space and reciprocal space. The former are (a/2, a/2,0), (-a/2, a/2, 0) and (0, 0, na) where n is the superlattice order. The latter are (1, 1, 0), (-1, 1, 0) and (0, 0, 1/n) in units of $2\pi/a$. Note that the vectors point in the same directions in both spaces. The advantage of the tetragonal setup is that one of the lattice vectors can be chosen to coincide with the superlattice axis (our z-axis), and elongation of the unit cell can be achieved by simple scaling of this lattice vector, leaving the other two unchanged. The same process would necessitate tedious recalculation of all three vectors if an fcc lattice were employed.

Figure 6.4.(c) shows the irreducible wedge of the tetragonal Brillouin zone. The symmetry points are (in reduced coordinates) :

Γ 000 X $0\frac{1}{2}0$ M $\frac{1}{2}\frac{1}{2}0$ Z $00\frac{1}{2}$ R $0\frac{1}{2}\frac{1}{2}$ A $\frac{1}{2}\frac{1}{2}\frac{1}{2}$

Because the number of atoms in the unit cell is double that of the

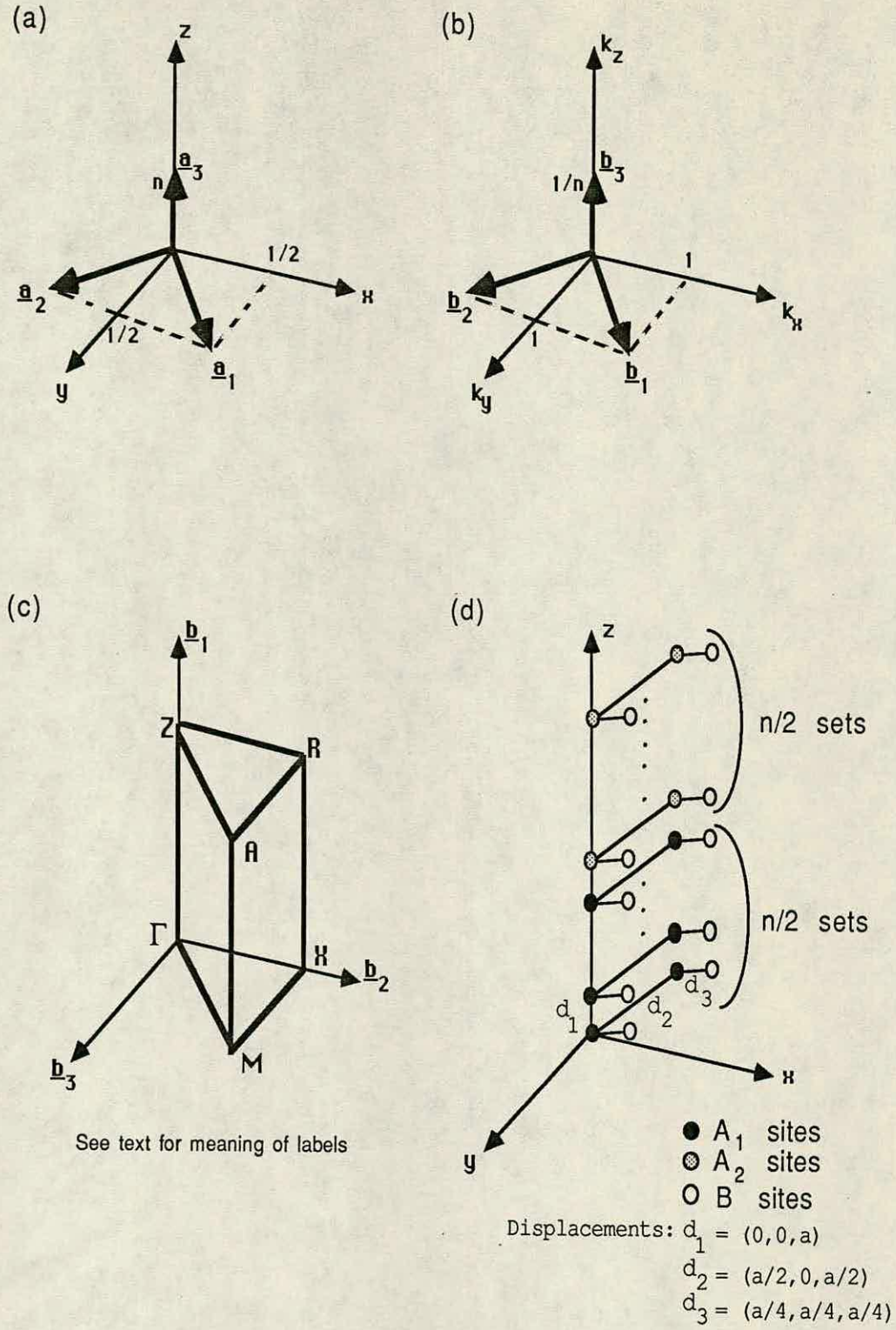

Figure 6.4. (a) Real space lattice vectors ; (b) reciprocal lattice vectors ; (c) irreducible wedge of the Brillouin zone ; (d) basis in real space (compressed in the z direction).

fcc setup, a general Cartesian point (α,β,δ) in the tetragonal zone represents the two points (α,β,δ) and $(\alpha,\beta,\delta+1)$ in the fcc zone. For example, $\Gamma_{tet}(000)$ maps to $\Gamma_{fcc}(000)$ and $X_{fcc}(001)$. The latter is just one of the 8 fcc X points. X_{tet} has no special fcc symmetry. $M_{tet}(\frac{1}{2}\frac{1}{2}0)$ becomes (010) in Cartesians, which maps to $X_{fcc}(010)$ and the point (011); however, the latter is equivalent to $X_{fcc}(100)$ via translation through the fcc reciprocal lattice vector (111). The Z point has the same symmetry in both systems. $R_{tet}(0\frac{1}{2}\frac{1}{2})$ includes the symmetry of $L_{fcc}(\frac{1}{2}\frac{1}{2}\frac{1}{2})$. Along X_{tet}-M_{tet} the pairs of fcc **k** vectors turn out to be equivalent, hence the observed twofold degeneracy in the tetragonal bands there.

Figure 6.4.(d) shows the basis (in real space), which consists of 4n atoms/ions. In the case of bulk III-V materials the Group III ions (e.g. Ga or Al) occupy the sites labelled A_1 and A_2, and the Group V ions (e.g. As) those labelled B. In the case of the $(GaAs)_n(AlAs)_n$ superlattice the n A_1 sites are occupied by Ga ions and the n A_2 sites by Al ions. Thus the unit cell always represents a cross-section of two layers, which is also the smallest possible unit of replication. This allocation of ions to A_1 and A_2 sites corresponds to stacking in the (001) direction.

Before presenting my results, we look at the results obtained by BK. Using their own norm-conserving pseudo-potentials, they obtained selfconsistent bandstructures for GaAs and AlAs and for the monolayer superlattice. These are shown from top to bottom in Figure 6.5. The labelling of the symmetry points and lines is relative to the tetragonal system and follows

(a)

(b)

(c)

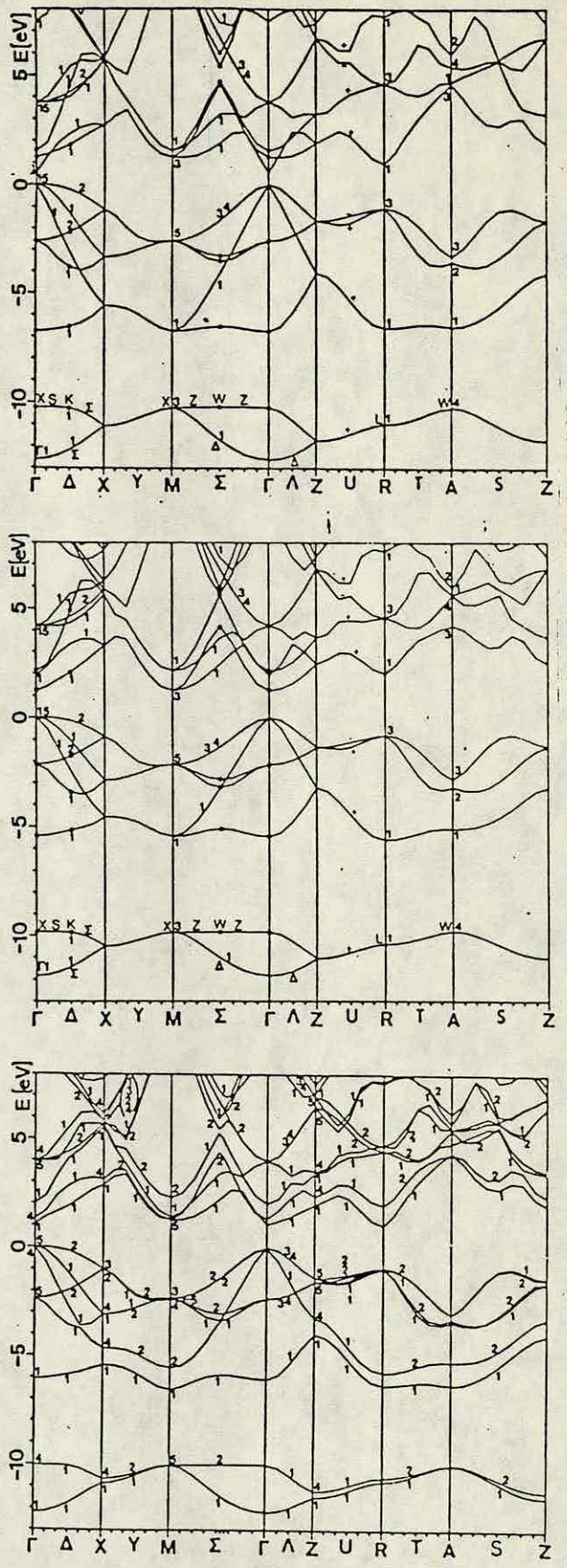

Figure 6.5. Bandstructures obtained by Bylander & Kleinman (1986) : (a) GaAs ; (b) AlAs ; (c) $(GaAs)_1(AlAs)_1$

that of Lax (1974). As expected, the bands for the two bulk compounds are very similar, especially the valence bands. The gaps exhibit the usual large LDA error (see Table 6.2). The alloy bands are intermediate between those of GaAs and AlAs, but with all the degeneracies split. There are also repulsions, where bands which previously crossed are no longer permitted to do so due to acquisition of the same symmetry. Finally we note that due to the effective doubling of the unit cell (and halving of the Brillouin zone) in the Z direction, the Γ-Z bands are equivalent to standard fcc Γ-X bands (see e.g. Chelikowsky & Cohen, 1976) which have been folded about their midpoint, thus doubling their number.

Figure 6.6 shows my bandstructure for GaAs along the same lines of symmetry as BK, omitting A-Z. A kinetic energy cutoff corresponding to a basis of around 300 plane waves is used (the exact number varies throughout the Brillouin zone because the kinetic energy is **k**-dependent), and the Lanczos algorithm is stopped after 64 steps. The valence bands are topologically in good agreement with BK. This is especially pleasing when one takes into account the potential superiority of the BK self-consistent calculation. The situation with the conduction bands is less satisfactory; indeed most of them are missing altogether. Taking the Lanczos algorithm further does not improve the situation because the disease is the use of REAL*4 precision. It should be clear from the upper reaches of Fig. 5.3 that the higher bands are unlikely to converge. The only remedy for this, as discussed in chapter 5, is REAL*8 precision, or possibly even algorithm enhancements such as selective orthogonalisation. One

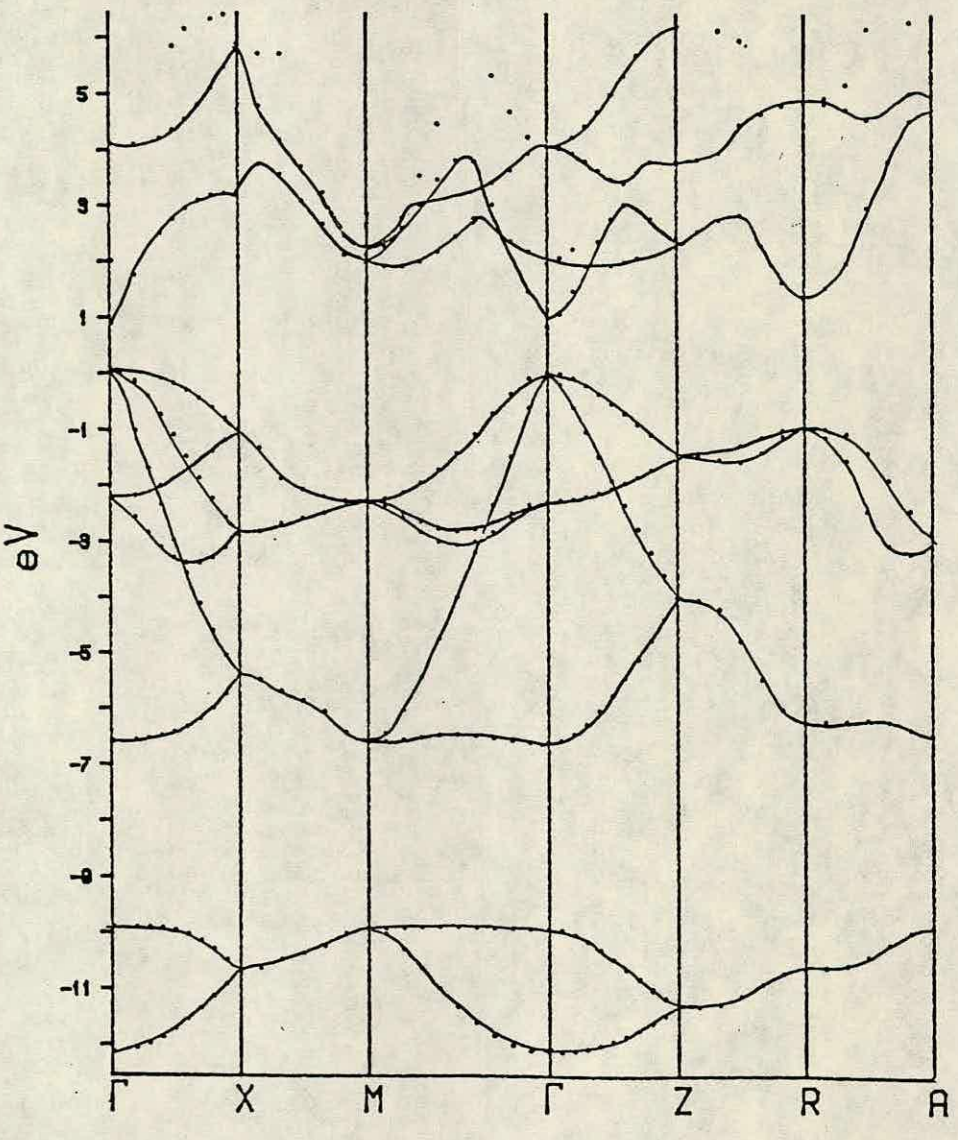

Figure 6.6. Calculated bandstructure of GaAs

	GaAs	AlAs	$(GaAs)_1(AlAs)_1$
Γ-Γ	0.83 , 0.544 , 1.425	2.2 , 1.910 , 2.95	1.05 , 1.043 , 2.095
X-Γ	2.1 , 1.248 , 1.911	2.0 , 1.245 , 2.168	1.8 , 1.259 , 1.975
L-Γ	1.5 , 0.948 , 1.734	2.45 , 2.003 , 2.363	1.0 , 1.024 , 2.021

Table 6.2. Energy gaps (with fcc labelling) in eV. Each triplet consists of my gap, the BK gap and the expt. gap (quoted by BK) in that order. The minimum gaps are on the diagonal of the table.

of the two lowest conduction bands along Γ-X is missing, but by good fortune it is its companion which determines the energy gap, being the lower of the two. This gap is tabulated in Table 6.2. It is about 70% of the experimental gap, which is better than the 40% achieved by BK. This is only to be expected as the latter (like my calculation for AlAs in section 3.3., which got 60% of the correct gap) contains an inherent error in the form of the LDA. What is perhaps surprising is that the fitted potential I use cannot yield a better gap.

Figure 6.7 shows the bandstructure obtained for AlAs. The comments are similar to those for GaAs, even extending to the energy gap. Good fortune has come to our aid again since although the lowest conduction band along Γ-X is missing, AlAs is actually an indirect gap material, the smallest gap being that between Γ and M (which is equivalent to the X point in the fcc system). The value I obtain for this (see Table 6.2) is very close to the experimental value of 2.17 eV (Lee et al.,1980). The BK value is 55% of this.

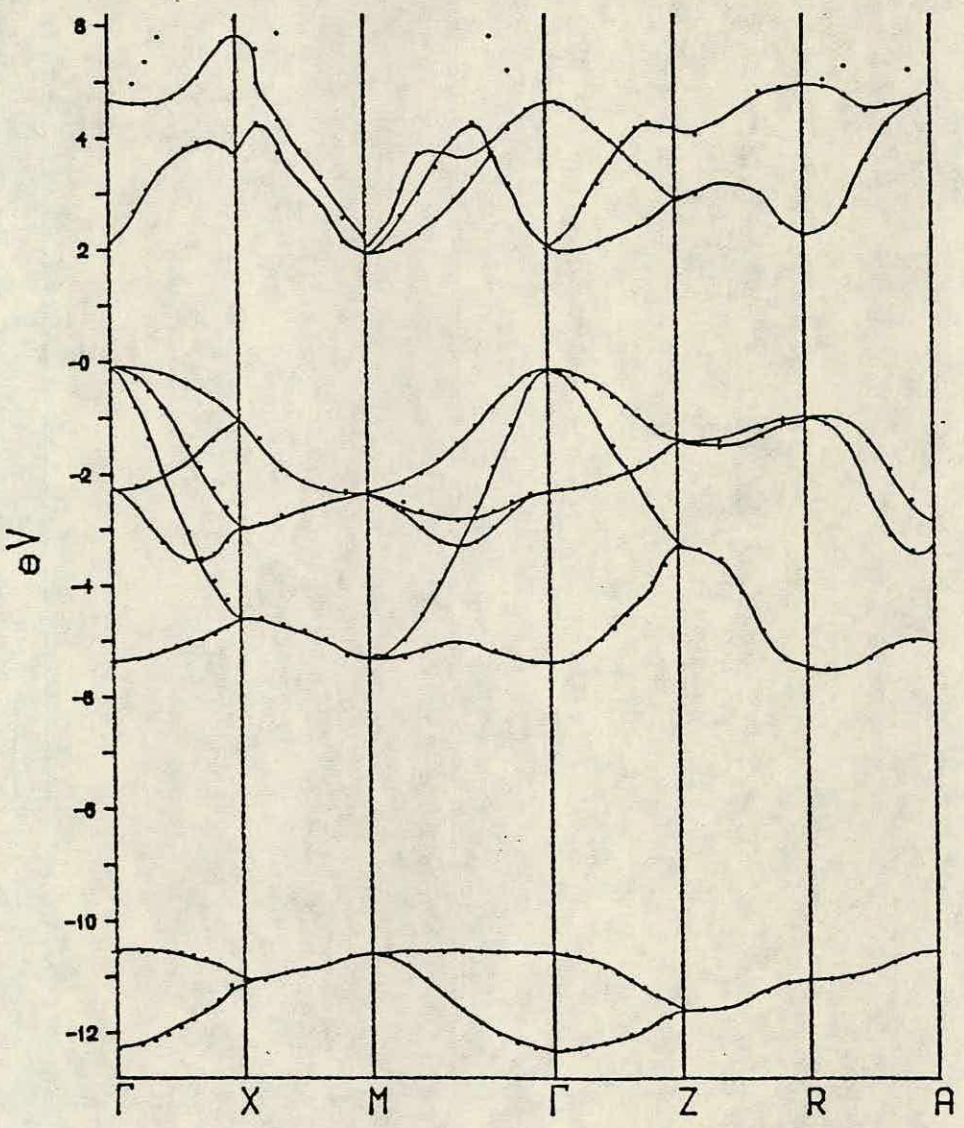

Figure 6.7. Calculated bandstructure of AlAs

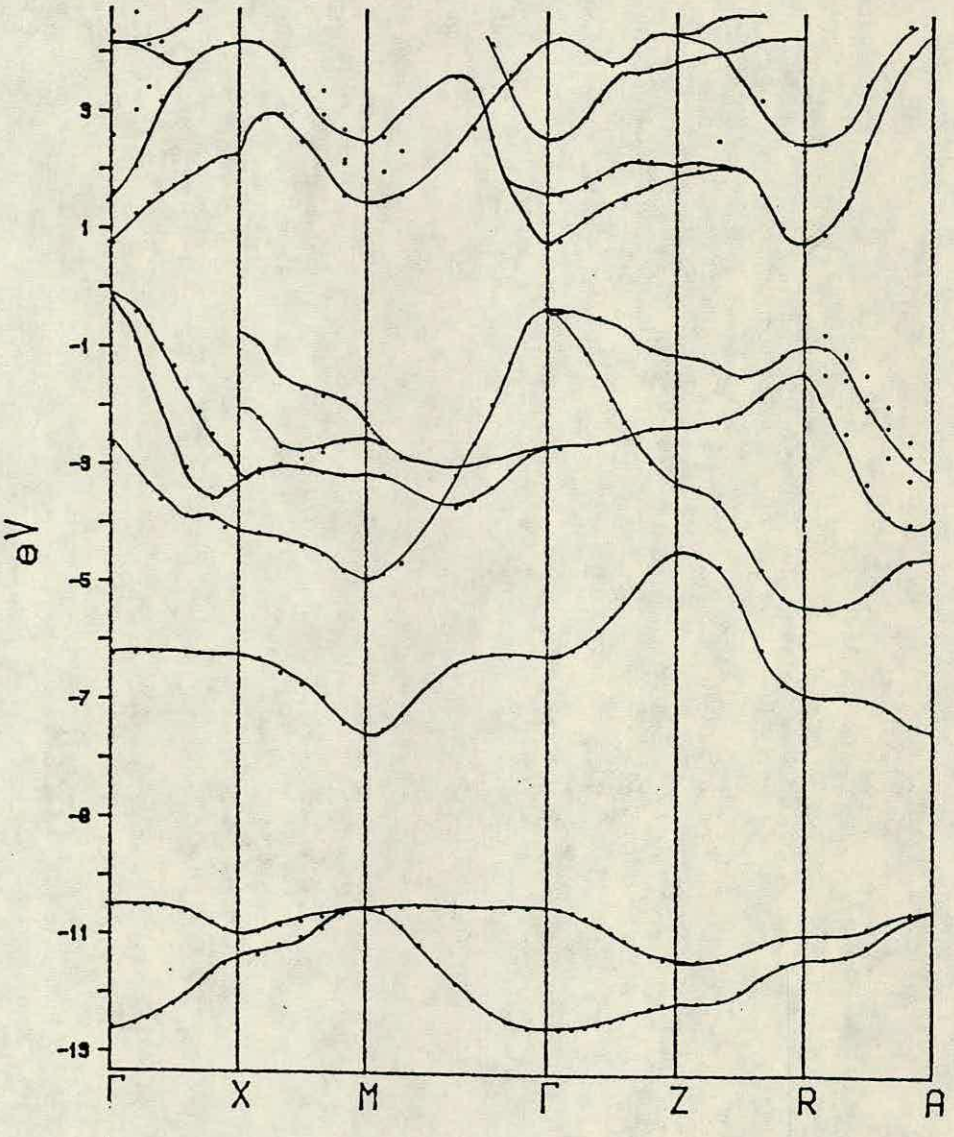

Figure 6.8. Calculated bandstructure of $(GaAs)_1(AlAs)_1$

Figure 6.8 shows the bandstructure calculated for $(GaAs)_1(AlAs)_1$. Here we enlarge the basis to 500 plane waves, while still terminating the algorithm after 64 steps. This results in the disappearance of a few of the valence bands, as well as of conduction bands. However, the bands we do have are in general topological agreement with the BK result in Figure 6.5. In this system BK and other workers (notably Nakayama & Kamimura) recently showed that the mimimum gap is between Γ and R (the fcc L point), and my result is not inconsistent with this. If my conduction band at Γ is indeed slightly lower than that at R, this is explicable by the lack of sensitivity in my potential. Earlier empirical calculations have completely failed to pick up the minimum gap at R.

While still on the subject of the n=1 system, we look at the $GaAlAs_2$ random alloy. We average the Ga and Al potentials on a 50/50 basis at all of the A_1 and A_2 sites. The bandstructure is shown in Figure 6.9. The valence bands exhibit no splitting of degeneracies and are similar to those of a bulk material, which is to be expected because there is no macroscopic heterogeneity in random $GaAlAs_2$ — it is a quasi-bulk material. The surprising feature of Figure 6.9 is the negative gap, a characteristic of a semimetal. This cannot be correct, as experiment shows $GaAlAs_2$ to be a semiconductor. It is unlikely to be connected to the fact that the random alloy is not energetically favoured, since the heat of formation of the ordered superlattice, although negative, is very small (BK obtained -9 meV), and so the alloy can easily

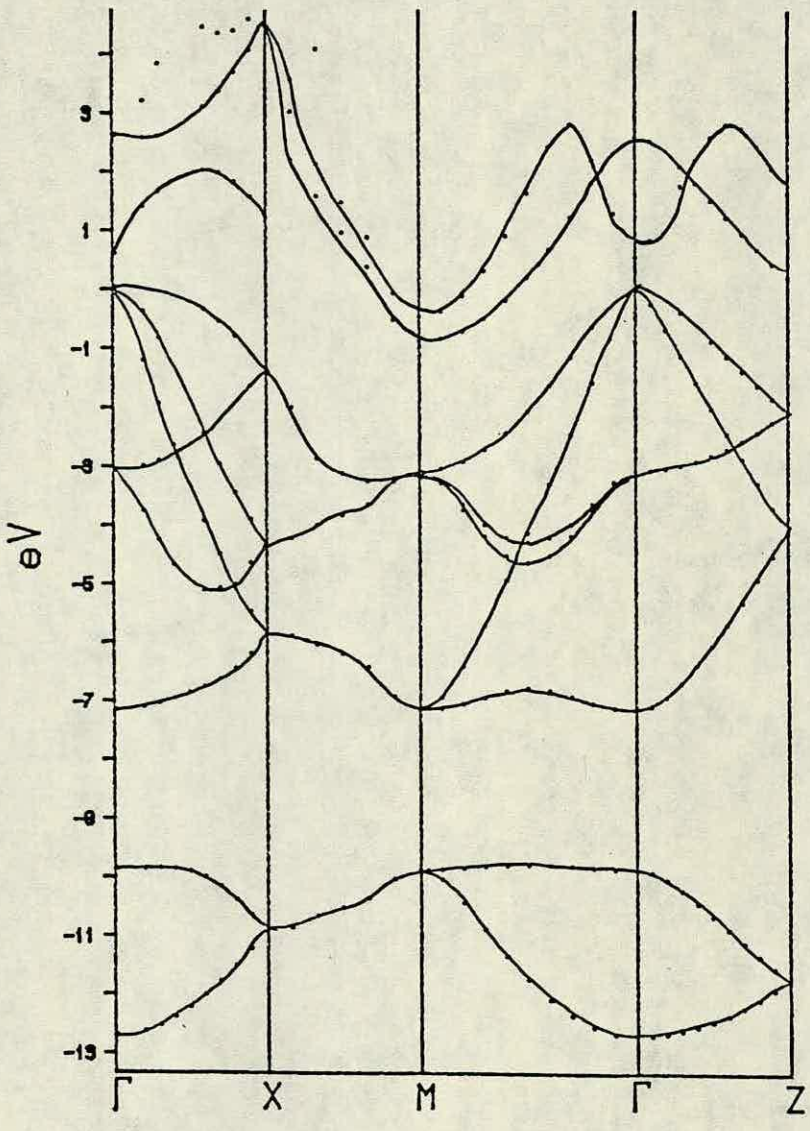

Figure 6.9. Bandstructure of the random alloy $GaAlAs_2$

exist at room temperature. In the absence of any other explanation we must conclude that the negative gap is simply due to an unfortunate synergy between the shortcomings of the three PLC potentials. The inadequacy of our Ga/Al averaging may also play a role; it would be of interest to try genuinely random assignments at each site, but this would require a large number of atoms in the unit cell to be statistically significant.

We now move on to discuss the true superlattices (those with $n > 1$), which involve elongation of the unit cell (and corresponding reduction of the Brillouin zone). The results for n=2 and n=4 are shown in Figures 6.10 and 6.11. Due to time constraints, these cover only Γ-M-X-Γ. In the case of n=2, dashed lines representing the likely valence bands on Γ–Z (unfortunately omitted from my calculation) have been sketched in such a way as to resemble the bands obtained by Nakayama & Kamimura (1985) for this section. Although the R point was seen to be of importance for n=1, this is not so for thicker-layered systems, all of which are expected (from experimental knowledge) to have direct gaps. In the case of n=4 we note that a somewhat finer mesh over the Brillouin zone would be needed to resolve the valence bands properly. Apart from the gaps (transferred to Figure 6.12), the only other feature worth commmenting on is the phenomenon of folding (e.g. Miller et al., 1981), which occurs in the direction of layer stacking (i.e. k_z) due to the shortening of the Brillouin zone in that direction. It is therefore present only on the projected Γ-Z section of our n=2 bandstructure (Fig. 6.10). According to Fig. 6.4.(c), folding would also occur on M-A and X-R, but we do not

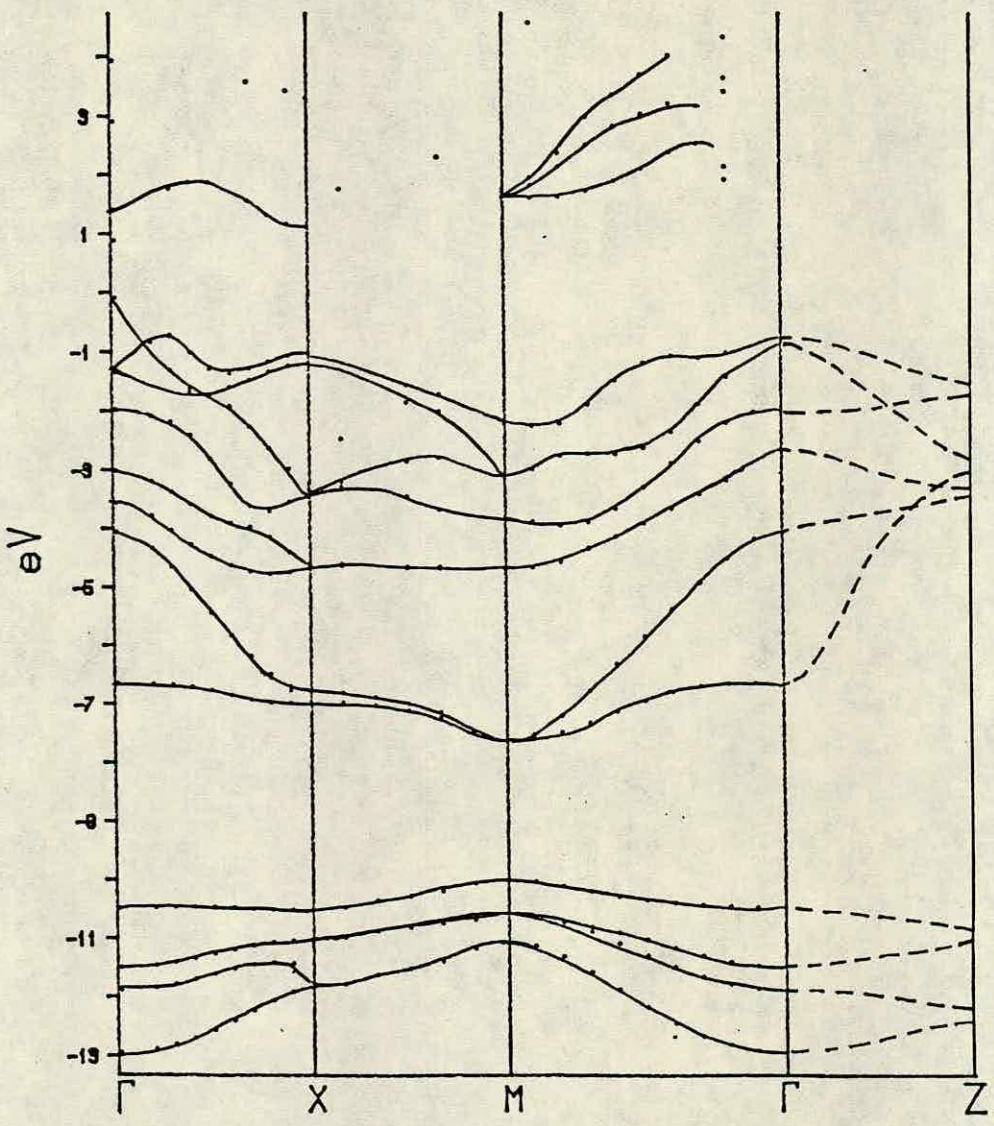

Figure 6.10. Calculated bandstructure of $(GaAs)_2(AlAs)_2$

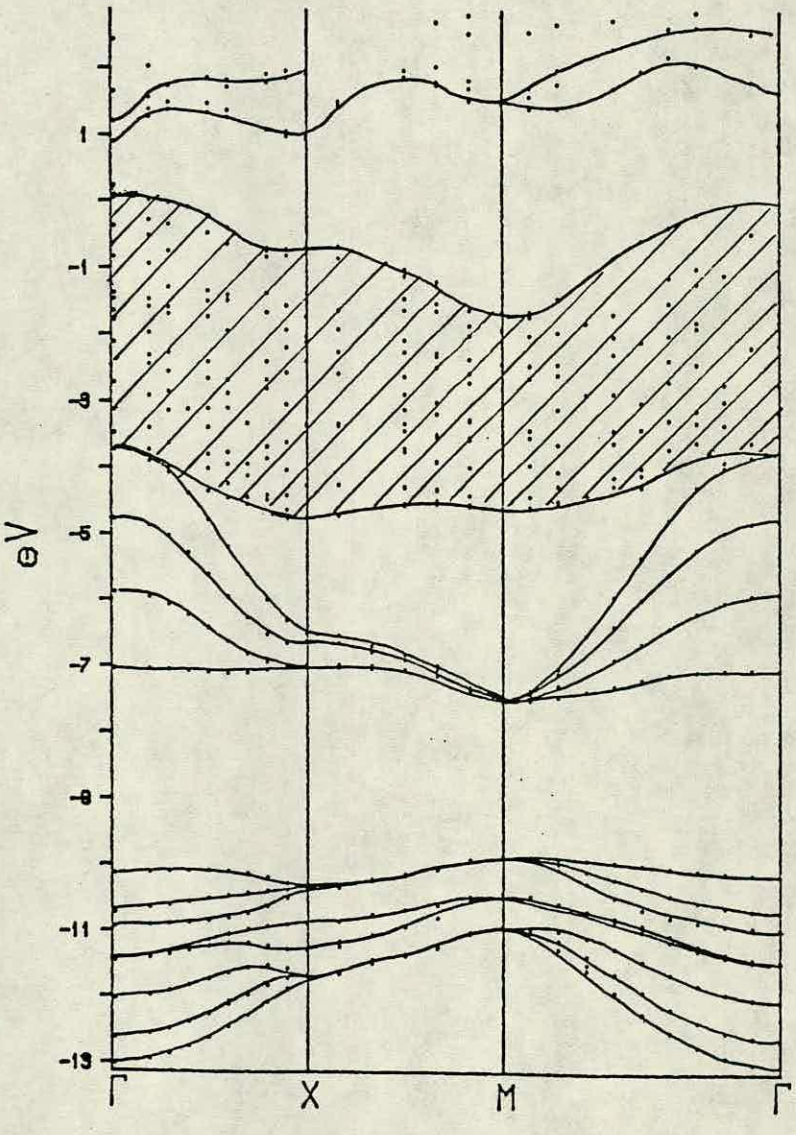

Figure 6.11. Calculated bandstructure of $(GaAs)_4(AlAs)_4$

calculate or show these. Comparison with the Γ-Z section for n=1 (Fig. 6.8) indicates that the right half of the n=1 bands get reflected ("folded") about the midpoint of that section. New gaps also open at the zone edges, since folded bands usually repel each other. In this way the concept of folding supplies the link between the minibands outlined in section 6.1 and the E versus **k** bandstructures we are calculating. The new gaps correspond to the gaps between real space minibands.

Our final set of results (Figure 6.12) shows the variation of energy gap against n, both from experiment (Ishibashi et al., 1985) and from three calculations, including mine. I estimate the gaps at n=5 and 6 from runs at Γ and a couple of nearby points. The selfconsistent work of Ferraz & Srivastava (1986) uses parametrised empirical potentials and is similar to what I had been hoping to achieve, the only major difference being that they used X-α screening whereas I would probably have used the LDA. Their agreement with experiment is good, as is that of the non-selfconsistent Jaros method (Gell et al. 1986) although the latter made use of judicious manipulation of the potentials. The gap variation I obtain is reasonably good, apart from the jump from n=1 to 2 (shared with Jaros). The absolute values of my gaps are about half the correct ones. This discrepancy is caused by the lack of selfconsistency and the flaws in the PLC potentials. It seems likely that the former contributes most of the error, since the individual potentials have been fitted to correct bandstructures, and it is unlikely that combining three of them could diminish a gap by 50% from its correct value.

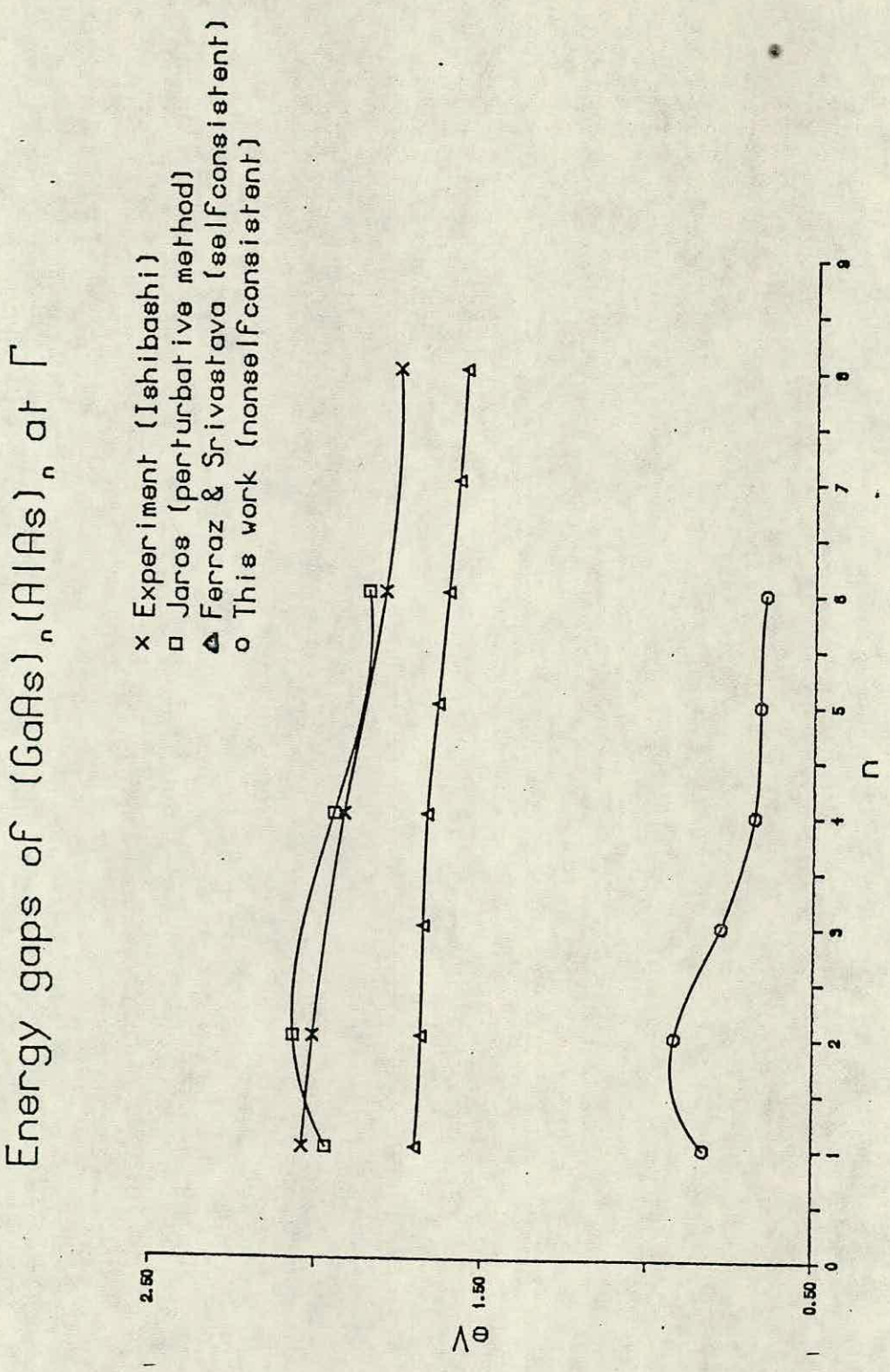

Figure 6.12. Variation of the energy gap

We close this chapter by drawing attention to our omission of spin-orbit coupling between s and p states, which would split the degeneracies in the valence bands at Γ and is therefore of importance for applications related to optical transitions. The Jaros group include spin-orbit coupling in their calculation (Gell et al. 1986). Tight-binding bandstructures for $(GaAs)_1(AlAs)_1$ with and without spin-orbit coupling have been presented by Jaffe and Singh (1987). They find the splitting at the top of the valence band to be around 0.4 eV, which is significant. Their gap is correspondingly decreased, but the rest of the bandstructure is virtually unchanged by the inclusion of spin-orbit coupling.

7. CONCLUSION

We conclude by stating the two principal problems with our calculation, from the standpoint of physics - as opposed to numerical analysis, into which field the Lanczos algorithm problems fall.

(1). The PLC potentials are inaccurate at small q, which happen to be the wavevectors that become important on moving from a bulk system to a periodic heterostructure.

(2). Selfconsistency is crucial for electronic structure calculations involving interfaces, or indeed any heterogeneity. There could be no better illustration of this than Figure 7.1, which is actually taken from PLC's paper. Being the same both at interfaces and far from them, the empirical potential does not

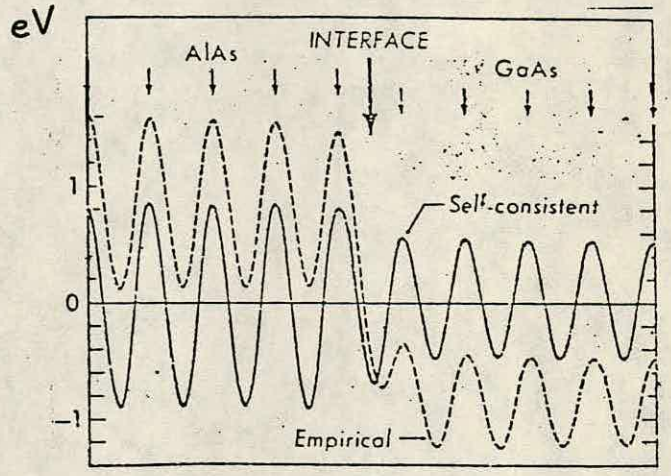

Figure 7.1. Empirical & selfconsistent potentials at GaAs/AlAs interface.

"know" about the interface(s) and cannot aspire to describe the situation until it has been taken to selfconsistency. The total charge density must "see" the nonuniform arrangement of ions and adjust itself accordingly.

Regarding future work, the obvious next step would be to migrate to a computer with sufficient memory (> 8 Mbytes) for REAL*8 arithmetic and the calculation of wavefunctions. This would enable self-consistent calculations, at least with local pseudopotentials. A shift to nonlocal potentials would demand further systematisation of coding techniques, perhaps taking the rudimentary method of Kleinman & Bylander as a starting point.

Finally, we suggest how related application areas may be affected by the parallel Lanczos algorithm. A major criticism of simple bandstructure calculations such as those performed in this thesis is the dearth of physical insight they provide. They suffice for the routine calculation of various material properties (such as the long list which appears on page 1 of the Introduction), but the overall cause of materials science would be carried further by gaining an understanding of the processes which make the bandstructure the way it is, and endow the material with the properties it has. A good response to this challenge is to perform Jaros-type perturbative calculations, where the basis functions are themselves electron states and the sizes of the matrix elements give the strengths of interaction, or mixing, between various states. The correlation of this sort of information with the bandstructure and properties should provide

fertile soil for predictions for more complex materials. At present workers in this area (e.g. Gell et al., 1986) use only crude potentials and small numbers of basis functions, but it seems certain that the desire to use more sophisticated potentials and study more complex systems will eventually lead to very large matrices. The parallel Lanczos algorithm I have described here will then be useful, as long as the potentials used are local.

An area where not the whole fast Lanczos algorithm, but its key element, the FFT speed-up, is finding application is the Car-Parrinello molecular dynamics technique mentioned in Section 2.1., which uses the trick as I do, to circumvent a very large matrix-vector multiplication (Allan & Teter, 1987). It seems possible that this method's latent capability to give a complete description, including crystal geometry, of any material will enable it (or some descendant of it) to eventually supersede all other electronic structure methods. If so, it is heartening to think that at least one component of this thesis will survive in some form for a long time.

APPENDIX

The fast Lanczos routine

This section gives the actual DAP subroutine DAPFLAN16, written in DAPFORTRAN. This version uses a 16^3 FFT routine, and is shorter and clearer than the one which uses 32^3, because the latter stores each vector over eight matrices to the former's one. The coding of the algorithm is consistent with (4.11) and Figure 4.1. Since the host code is not listed here, we first briefly outline the actions it performs. In addition, an index for the DAP code follows its listing. The MERGE function is defined in Section 5.1.

The host sets up the potential in Fourier space (on the 1st **k**-point of the run only; the DAP passes V(r) out again for future **k**-points) and the two **k**-dependent entities, the kinetic energy and the mask expressing the basis as a subset of the FFT grid. Apart from the basis size NK (max. 4096 in this version), there is another important user-chosen parameter, the number of Lanczos cycles ICYC which is typically 100-400. If ICYC is to be of order 500 or more (as a result of NK >> 1000), the number of eigenvalues of T_J actually found by the library routine would need to be increased from its present fixed level of 64 (which is also the maximum for the routine, so that would have to be modified). The sorting of the raw Lanczos output into genuine eigenvalues, ghosts and spurious eigenvalues (by comparison of the results from T_{61}, T_{62}, T_{63} and T_{64}) was originally done in the DAP using logical masking. But this proved difficult to monitor and debug, so was moved to the host, where it follows the call to DAPFLAN16.

Listing of the DAP code

```
          ENTRY SUBROUTINE DAPFLAN16
C--Low energy bands using parallelised Lanczos algorithm.
C--Donald Macleod--Edinburgh University--January 1987
          REAL*8 WR,WI,VR,VI,EK,ALPHA,BETA,ENER
          REAL*8 QR(,),QI(,),XR(,),XI(,),TEMP(,)
          INTEGER*4 BMASK
          INTEGER*4 IEIG()
          COMMON/WORKSPACE/WR(,),WI(,)
C--following blocks are INPUT from the host:
          COMMON/POT1/VR(,)
          COMMON/POT2/VI(,)
          COMMON/MASK/BMASK(,)
          COMMON/EKIN/EK(,)
          COMMON/PARAM/NLANC,NK,IFAIL,ITER,IKP,ICYC
C--following blocks are OUTPUT to host; also POT1,POT2,PARAM:
          COMMON/ALP/ALPHA(,)
          COMMON/BET/BETA(,)
          COMMON/EVAL/ENER(,)
C--conversion to DAP storage format .
          CALL CONVFM8(VR)
          CALL CONVFM8(VI)
          CALL CONVFM8(EK)
          CALL CONVFMI(BMASK)
          CALL CONVFSI(NLANC,6)
C--initialisation
          QR = 0.0
          QI = 0.0
          XR = 0.0
          XI = 0.0
          DO 5 I = 1,64
     5    IEIG(I) = I
C--set first Lanczos vector to (1,0,0,...0); NLANC option omitted.
          QR(1,1) = 1.0
C--if at first k-point transform V(G) to V(r) once and for all;
C--VR,VI get overwritten by transformed potential.
          IF (IKP.EQ.1) CALL FFT16CB(VR,VI,.TRUE.,.TRUE.)
C--start of actual Lanczos loop (ends line 100).
          DO 100 J = 1,ICYC
          IF (J.EQ.1) GOTO 50
          TEMP = QR
```

```
            QR = XR/BETA(J)
            XR = -TEMP*BETA(J)
            TEMP = QI
            QI = XI/BETA(J)
            XI = -TEMP*BETA(J)
C--transform Lanczos vector to q(r).
     50     WR = QR
            WI = QI
            CALL FFT16CB(WR,WI,.TRUE.,.FALSE.)
C--form the product V(r)q(r) and transform it to Σ_G'V(G-G')q(G).
C--VI is assumed to be zero.
            WR = WR*VR
            WI = WI*VR
            CALL FFT16CB(WR,WI,.FALSE.,.FALSE.)
C--add K.E. & mask out convolution elements with G's not in basis.
            XR = XR+EK*QR+MERGE(WR,0.0,BMASK.EQ.1)
            XI = XI+EK*QI+MERGE(WI,0.0,BMASK.EQ.1)
C--find J'th α and β ; index of β shifted by 1 for eigval. routine.
            ALPHA(J) = SUM(QR*XR+QI*XI)
            XR = XR-ALPHA(J)*QR
            XI = XI-ALPHA(J)*QI
            TEMP = XR**2+XI**2
            BETA(J+1) = SQRT(SUM(T))
C--on last 4 cycles find lowest 64 eigenvalues of T_J (--> ENER) .
            IF (J.LT.ICYC-4) GOTO 100
            IFAIL = 0
            IEVAL = J-ICYC+5
            CALL DP_EIG_VALS_TD_4096(ALPHA,BETA,J,IEIG,64,
           *                                  ENER(,IEVAL),ITER,IFAIL)
    100     CONTINUE
C--convert output to host storage format
            CALL CONVMF8(VR)
            CALL CONVMF8(VI)
            CALL CONVMF8(ALPHA)
            CALL CONVMF8(BETA)
            CALL CONVMF8(ENER)
            RETURN
            END
```

Index

For arrays, the total number of elements is given in brackets.

ALPHA (4096) - main diagonal of T_J

BETA (4096) - off diagonal of T_J

BMASK (4096) - mask with 1 at every point of FFT grid corresponding to a **G** in the basis, 0 elsewhere.

DPEIGVALSTD4096 - tridiagonal eigenvalue solver from QMC DAP subroutine library (a parallelised version of F04EIGVALSTD4096 in NAG library), modified to REAL*8 by myself.

EK (4096) - vector of kinetic energies

ENER (4096) - eigenvalues. Only the first 4 columns get filled.

FFT16CB - 3-dimensional fast Fourier transform on a 16^3 grid, written for the DAP by S. Sheard (1986). The first logical parameter is TRUE for a Fourier-to-real transform and FALSE for real-to-Fourier.

ICYC - the number of Lanczos cycles desired

IEIG (64) - the particular eigenvalues to be found (always 1-64)

IFAIL - error message from DPEIGVALSTD4096

IKP - the number of the **k**-point

ITER - the number of bisections DPEIGVALSTD4096 had to do

J - the Lanczos cycle dummy variable

NK - size of basis (max. 4096) ; not actually needed by DAP

NLANC - controls the choice of $\mathbf{q}_1$ (no choice in the listed version)

QR (4096) - real part of Lanczos vector

QI (4096) - imaginary part of Lanczos vector

TEMP (4096) - temporary storage

VR (4096) - real part of potential

VI (4096) - imaginary part of potential (Fourier space only!)

WR(4096) - workspace

WI (4096) - workspace

XR(4096) - workspace

XI (4096) - workspace

BIBLIOGRAPHY

Allan, D.C. , M.P.Teter Phys. Rev. Lett. 59 1136 (1987)

Bachelet, G.B., D.R.Hamann, M.Schluter Phys. Rev. B 26 4199(1982)

Barbour, I.M., N.E.Behilil, P.Gibbs, G.Schierholtz, M.Teper in The Recursion Method and its Applications (eds. D.G.Pettifor, D.L.Weaire; Springer Verlag, 1985)

Bauer, R., G.Margaritondo Physics Today (Jan. 1987) p.27

Brand, S., R.A.Abram J. Phys. C 16 6111 (1983)

Brass, A., G.S.Pawley Parallel Comput. 3 167 (1986)

Brigham, E.O., The Fast Fourier Transform (Prentice-Hall, 1973)

Bylander, D.M., L.Kleinman Phys. Rev. B 34 5280 (1986)

Car, R., M.Parrinello Phys. Rev. Lett. 55 2471 (1985)

Caruthers, E., P.J. Lin-Chung Phys. Rev. B 17 2705 (1978)

Ceperley, D., B.Alder Science 231 555 (1986)

Chadi, D.J., M.L.Cohen Phys. Rev. B 8 5747 (1973)

Chelikowsky, J.R., M.L.Cohen Phys. Rev. B 14 556 (1976)

Chelikowsky, J.R., D.J.Chadi, M.L.Cohen Phys. Rev. B 23 4013 (1981)

Ciraci, S., I.P.Batra Phys. Rev. Lett. 58 2114 (1987)

Cohen, M.L., V.Heine in Solid State Physics (eds. F.Ehrenreich, C.Seitz) 24 (1970)

Danielson, G.C., C.Lanczos J. Franklin Institute 233 365 (1942)

Döhler, G.H. Festkörperprobleme XXIII 207 (1983)

Esaki, L., R.Tsu IBM J. Res. Dev. 14 61 (1970)

Ferraz, A.C., G.P.Srivastava Semicond. Sci. Technol. 1 169 (1986)

Froyen S., M.L.Cohen Phys. Rev. B 28 3258 (1983)

Gell, M.A., D.Ninno, M.Jaros, D.C.Herbert Phys. Rev. B 34 2416 (1986)

Godby, R.W., M.Schluter, L.J.Sham Phys. Rev. Lett. 56 2415 (1986)

Godby, R.W., M.Schluter, L.J.Sham Univ. of Cambridge preprint (1987)

Golub, G.H., C.F.van Loan Matrix Computations (N.Oxford Academic, 1983)

Hamann, D.R., M.Schluter, C.Chiang Phys. Rev. Lett. 43 1494 (1979)

Haydock, R. in Solid State Physics (eds. F.Ehrenreich, C.Seitz) 35 (1980)

Hedin, L., B.I.Lundqvist in Solid State Physics (eds. F.Ehrenreich, C.Seitz) 23 (1969)

Hedin, L., B.I.Lundqvist J.Phys. C 4 2064 (1971)

Heine, V. in Solid State Physics (eds. F.Ehrenreich, C.Seitz) 24 (1970)
Hillis, W.D. The Connection Machine (M.I.T. Press, 1985)
Hohenberg, P., W.Kohn Phys. Rev. B 136 864 (1964)
Holonyak, M. et al. IEEE J. Quantum Elect. 16 170 (1980)
Householder, A.S. J. Soc. Ind. Appl. Math. 6 189 (1958)
Hurkx, G.A.M., W.van Haeringen J. Phys. C 18 5617 (1985)
Ishibashi, A., Y.Mori, M.Itabashi, N.Watanabe J. Appl. Phys. 58 2691 (1985)
Jaffe, M.D., J.Singh Sol. St. Comm. 62 399 (1987)
Jaros, M. Rep. Prog. Phys. 48 1091 (1985)
Kahan, W., B.Parlett in Sparse Matrix Computations (eds. Bunch, Rose) (Academic Press, 1976)
Kleinman, L., D.M.Bylander Phys. Rev. Lett 48 1425 (1982)
Kohn, W., L.J.Sham Phys. Rev. A 140 1133 (1965)
Koopmans, T. Physica 1 104 (1933)
Kuan, T.S., T.F.Kuech, W.I.Wang, E.L.Wilkie Phys. Rev. Lett. 54 201 (1985)
Lanczos, C. J. Res. Nat. Bur. Stand. 45 255 (1950)
Lax, M. Symmetry Principles in Solid State and Molecular Physics (Wiley, 1974)
Lee, H.J., L.Y.Juravel, J.C.Woolley Phys. Rev. B 21 659 (1980)
Löwdin, P. J. Chem. Phys. 19 1396 (1951)
MacDonald, A.H., S.H.Vosko J. Phys. C 12 2977 (1979)
Miller, A., A.Mackinnon, D.Weaire in Solid State Physics (eds. F.Ehrenreich, C. Seitz) 36 (1981)
Miller, D.A.B. et al. Appl. Phys. Lett. 45 13 (1984)
Mimura et al. Jpn. J. Appl. Phys. 19 L225 (1980)
Monemar, B. Phys. Rev. B 8 5711 (1973)
Monkhorst, H.J., J.D.Pack Phys. Rev. B 13 5188 (1974)
Nakayama, T., H.Kamimura J. Phys. Soc. Jpn. 54 4726 (1985)
Paige, C. BIT 10 183 (1970)
Parlett, B. The Symmetric Eigenvalue Problem (Prentice-Hall, 1980)
Parlett, B., D.S.Scott Math. Comp. 33 217 (1979)
Phillips, J.C., L.Kleinman Phys. Rev. 116 287 (1959)
Pickett, W.E., S.G.Louie, M.L.Cohen Phys. Rev. B 17 815 (1978)
Pickett, W.E., C.S.Wang Phys. Rev. B 30 4719 (1984)
Slater, J.C. Adv. Quantum Chem. 6 1 (1972)

Slater, J.C. The Self-consistent Field for Molecules and Solids
(Quantum Theory of Molecules & Solids, Vol. 4)
(McGraw-Hill, 1974)
Tersoff, J. Phys. Rev. B 30 4874 (1984)
Tersoff, J. Phys. Rev. Lett. 56 2755 (1986)
van de Walle, C.G., R.M.Martin Phys. Rev. B 34 5621 (1986)
Weast, R.C. Handbook of Chemistry & Physics 62nd ed.
(Chemical Rubber Company,1981)
Williams, G.P. et al. Phys. Rev. B 34 5548 (1986)